

Computational model on neuronal stabilization in perceptual choice dynamics

Master Thesis

Wessel Woldman
Applied Mathematics
Applied Analysis and Mathematical Physics
University of Twente
Enschede, The Netherlands

Supervisors:
Dr. H.G.E. Meijer
Prof. dr. S.A. van Gils
Prof. dr. R.J.A. van Wezel

Contents

1	Introduction	3
2	Literature visual perception	6
2.1	Psychophysics	6
2.2	Neurophysiological experiments	6
2.2.1	Results	7
2.3	Mathematical models	9
2.3.1	Noest	9
2.3.2	Stochastic drift-diffusion model	9
2.3.3	Wang and Wong	12
2.3.4	Laing and Chow	14
3	Methods	18
3.1	Simulating the model	18
3.2	Output measures	18
3.3	Validation	20
3.3.1	Distribution of dominance duration	20
3.3.2	Largest Lyapunov exponent	21
3.3.3	Second Level's proposition	23
3.4	On-off-structure	23
4	Results	25
4.1	Off-durations	25
4.1.1	Alternation	27
4.1.2	Repetition	27
4.2	Slow processes	28
5	Discussion	34
6	Appendix	38

1 Introduction

Percept switching during experiments with visual stimuli is a well-studied subject within psychophysics, neurophysiology and computational neuroscience [2, 21, 9, 24, 3]. Spontaneous switches can be triggered by different visual stimuli, such as ambiguous visual stimuli or binocular rivalry images. An ambiguous visual stimulus has multiple and equally plausible interpretations, such as the Necker cube (figure 1.1). During constant viewing of an ambiguous visual stimulus, perception naturally switches over time. A typical example of ambiguous visual stimuli in neurophysiological experiments consist of moving dots within a transparent circle or cylinder. Due to a mechanism called structure from motion (SFM) the two-dimensional stimulus is perceived as a 3-dimensional rotating object. MT (middle temporal) is a region of the visual cortex that is thought to play a major role in the perception of motion, the integration of local signals into percepts and the guidance of eye movements. Since these SFM-stimuli evoke neuronal activity in area MT, these stimuli enable recordings of neuronal responses during the perception of the stimuli.

During binocular rivalry experiments, the left and the right eye receive different input simultaneously. A typical example of stimuli that lead to binocular rivalry are orthogonal gratings (see figure 1.2). During the stimulus-presentation, only one of the two presented images is perceived, and the other image is suppressed. During constant viewing of a binocular rivalry stimuli, perception naturally switches over time. Dominance durations, the time a percept remains dominant, are typically in the order of several seconds and the dominance distribution is unimodal and skewed with a long tail at long durations [18].

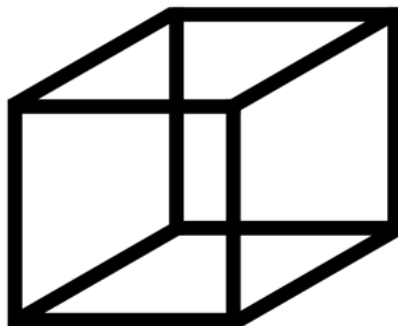


Figure 1.1: Example of an ambiguous visual stimuli: the necker cube has several equally plausible interpretations since the two-dimensional intersection allows several depth-configurations (crossing lines in two dimensions lead to ambiguity in three dimensions). During constant viewing, perception will typically switch between the two percepts although it should be noted subjects often have a preferred percept. These effects of learning or voluntary control might influence the switching.

Psychophysical and neurophysiological studies and experiments have resulted in a variety of neurocomputational models and approaches studying percept-sequences during steady viewing conflicting stimuli [24, 16]. In general, adaptation, a decrease in the responsiveness of a system to a constant stimulus, is attributed a key-role in inducing spontaneous percept switches. If after stimulus-onset one of the percepts gains dominance, it is hypothesized that adaptation will lead to a decrease in the responsiveness of the neurons corresponding to the

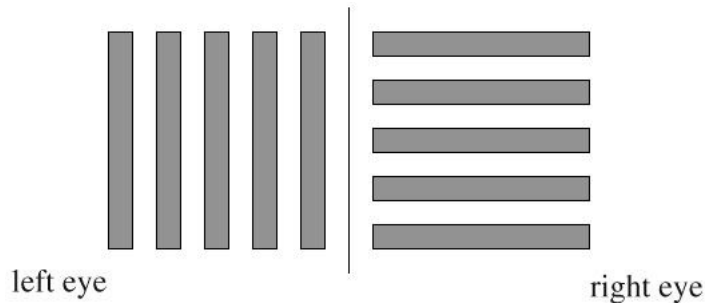


Figure 1.2: Example of a stimulus used in binocular rivalry experiments: orthogonal gratings. The left eye receives vertical gratings whereas the right eye receives horizontal gratings. During constant viewing, perception will switch between the two percepts.

coding of the dominant percept. Adaptation then eventually destabilizes the dominant percept, allowing the suppressed percept to gain dominance. In mathematical terms, this form of adaptation is described by regarding the two stable percepts as stable attractors. Since activity is directly correlated with one of the possible percepts and the attractors are both stable, there will be neural competition between the two percepts. As such, spontaneous percept switches are successfully understood (see for example figure 1b in Noest [24]) in terms of adaptation and noise [24].

These neural mechanisms leading to alternations during constant viewing do not explain what happens at the onset of the conflicting stimulus [24]. The question arises how the visual system chooses one of the options at stimulus onset. Several psychophysical and neurophysiological studies have approached this questions with a different stimulation-paradigm: instead of constant viewing, stimuli are now presented in interrupted sequences [24, 16, 3] with a certain on-duration (the duration the stimulus is shown) and off-duration (the time the stimulus is not shown).

These human psychophysical experiments have shown that percept sequences from interrupted stimulations are often more complicated than the alternating choice-sequence during constant viewing [24, 16]. At long inter-stimulus intervals, temporarily removing an ambiguous pattern leads to repetitions of the same percept. This phenomenon is called perceptual stabilization or perceptual memory. This suggests there is a different dynamical structure between spontaneous percept-switches and choice-sequences after stimulus onset. While it is currently unclear what happens inside the brain during perceptual stabilization, response characteristics might be influenced by other processes than adaptation.

A phenomenological approach by Noest in [24] provides a computational approach towards understanding percept-choice dynamics. It provides a connection between percept choices and spontaneous switches and furthermore explains in detail their fundamental different dynamical structure. By applying a mean-field approach, Noest has developed a phenomenological neurocomputational model in terms of activity and adaptation. The model consists of a set of non-linear differential equations in terms of average activity levels and average adaptation levels. The results match psychophysical findings and the model allows mathematical analysis [24]. Their model provides general insight in the processes and mechanisms underlying choice-percepts and the question arises whether these mechanisms and processes can be explained at the neuronal level.

A recent study by Klink in [17] investigated neuronal response patterns during intermittently presented ambiguous visual stimuli. During Klink’s experiments, awake macaque monkeys are presented with different types of visual stimuli and their neuronal responses were measured during intermittently presented sequences of stimuli. Statistical analysis of the responses suggests *neuronal stabilization*: a decrease of across-trial neural variability in responses for longer off-durations. Since Klink’s neurophysiological data-set consists of spike times and local field potentials, it is natural to consider neuronal network models, since these models might connect the micro-level of the neuronal data with the macro-level of the perception through mathematical analysis. Recent studies by Wang and Wong in [28] and Laing and Chow in [18] provide such starting points.

Laing and Chow’s neuronal network represents a higher-level of visual cortex such as LIP (or MT [18]). These areas receive input from lower-level areas. Activity in higher-level areas is typically more correlated with the percept than is the case for lower level areas [20]. Neurons can be either excitatory or inhibitory and are based on Hodgkin-Huxley-dynamics. When two conflicting stimuli are presented, the network is unable to sustain activity centered around both inputs simultaneously. As a result, activity alternates between one focus of activity and the other. This switching is the neurophysiological correlate of binocular rivalry, caused by two slow processes, spike frequency adaptation and synaptic depression. Spike frequency adaptation reduces the frequency of rhythmic tonic firing, and sometimes terminates the firing. Synaptic depression is a form of short-term input-specific plasticity exhibited by many synapses. Their model reproduces several psychophysical findings of studies of binocular rivalry [18].

We focus on developing a neuronal network model that allows us to connect the human psychophysics experiments in [24, 16] with the new neurophysiological data-set in [17] through a mathematical model. We first will discuss several phenomenological and neurobiological computational models describing perceptual choice dynamics. We will argue that since the human psychophysics studies by Noest and Klink showed their results and conclusions hold for both ambiguous stimuli and binocular rivalry stimuli, we can take the approach by Laing and Chow for binocular rivalry as a starting point for our neuronal network. Before we include the on-off-structure in the Laing and Chow model, we will first test our basic version of the Laing and Chow model against their three main results (distribution of dominance durations, largest Lyapunov exponent and second Levelt proposition). We then include the on-off-paradigm and explore the model’s behavior over a wide range of values for the on-durations and off-durations. We will show our on-off-network model provides a connection with the human psychophysics experiments by Klink and Noest in [16, 24] and allows spike-train analysis as in Klink [17]. We will argue the calcium-evolution is the main candidate key-player in understanding percept choice at the onset of stimuli. Although a reduced approach and bifurcation-analysis were not directly applicable to determine qualitative insight in the calcium-dynamics, this is a crucial and interesting question for future work. Our model can function as a basis for neurobiological experiment, such as calcium-imaging. Such experiments can hopefully guide the process of bridging the gap between the macro-scale of perception and micro-scale of neuronal responses during sequential stimulation with conflicting visual stimuli.

2 Literature visual perception

Since we want to develop a neuronal network model for repeated sequences of visual stimuli that connects to psychophysics, neurophysiology and neurocomputational models, we will first discuss the human psychophysical results that led to the development of mathematical models and neurophysiological experiments. We will then present an overview of the important different mathematical approaches that reproduce the psychophysical results and as such present possible explanations of the underlying neural mechanisms.

2.1 Psychophysics

During human psychophysics experiments with intermittently presented conflicting stimuli (figure 2.1), it was found that choice-sequences depend crucially on the length of the off-duration [24, 16]. The off-duration determines whether perception stabilizes (choice sequence: A, A, A...) or alternates (choice sequence: A, B, A...), and these effects are found approximately independent from the on-duration. Alternations typically occur for relatively short off-durations ($< 0.5s$) whereas repetitions emerge for longer off-durations ($> 0.5s$). The effects during increasing off-durations were found both during the rotating sphere and the orthogonal gratings. Since this suggest an underlying neural mechanism in the visual system during perception of conflicting stimuli, neurophysiological studies that record neuronal responses during the same stimulation-paradigm provide a starting point for investigating this neural mechanism.

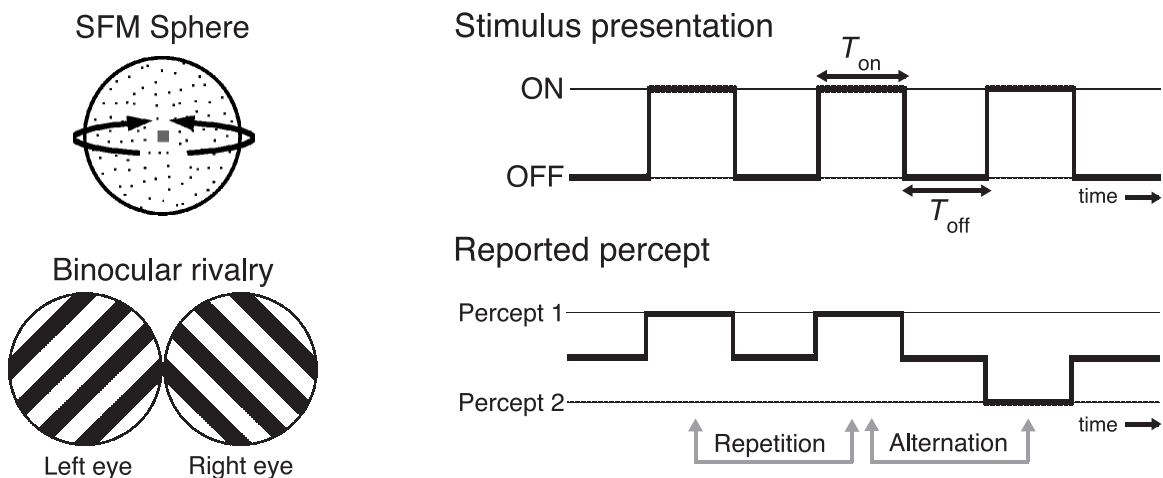


Figure 2.1: Stimulation paradigm in human psychophysics experiments by Klink in [16]. Stimuli were intermittently presented with a fixed on-duration and a fixed off-duration that was varied over blocks of trials. During the on-duration, the subject reported the current perceived percept (from [16]).

2.2 Neurophysiological experiments

A recent neurophysiological study by Klink analyzed the underlying neuronal mechanisms during repetitive stimulation (figure 2.2) of visual stimuli [17]. To investigate the neuronal

activity during perceptual stabilization, electrodes were placed in the motion-sensitive brain area (MT) of two awake macaque. In total 94 single units were used, recording spike-trains and local field potentials (LFP). In addition to ambiguous rotating cylinders, two non-ambiguous stimuli were included as control-groups, with the same stimulation-paradigm (figure 2.3). Klink hypothesized that if MT-neurons participate in encoding visual stimuli and if longer off-times lead to perceptual stabilization, then neuronal response patterns of the MT-neurons should stabilize accordingly.

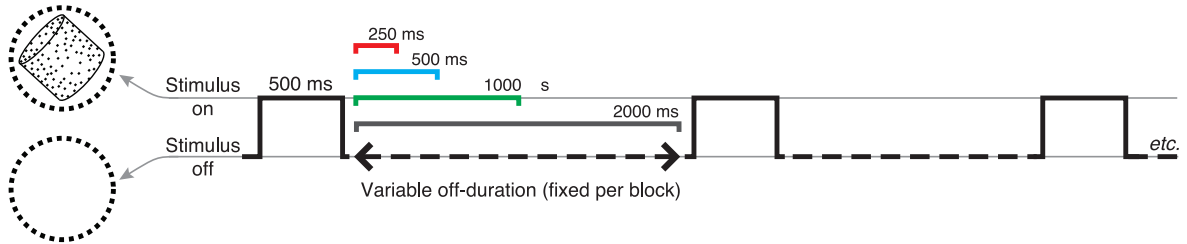


Figure 2.2: Stimulation paradigm in neurophysiological experiments by Klink in [17]: stimuli were placed in a neuron’s receptive field during experiments. Stimuli were intermittently presented with a fixed on-duration of 500 ms and a variable off-duration that was varied over blocks of trials between 250, 500, 1000 and 2000 ms. During the off-durations no stimulus was presented and neuronal responses were measured during the entire sequence of trials. The experiments consisted of sequences of 80 trials and within a sequence of 80 trials, the on- and off-duration were fixed and the neuronal activity was recorded during the entire sequence (from [17]).

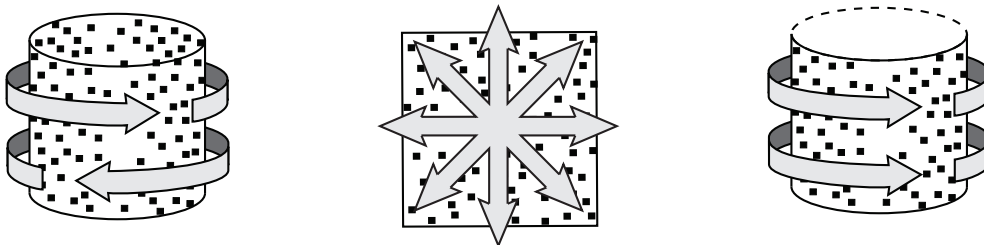


Figure 2.3: Stimuli in [17]. (left): an ambiguous structure-from-motion (SFM) cylinder stimulus, (middle): a dynamic random dot pattern (coherence 0%) with random starting position on every presentation, and (right): an opaque SFM cylinder, similar to the ambiguous cylinder, but only the dots that moved in the neuron’s preferred direction were presented on the screen (from [17]).

2.2.1 Results

For all three stimuli, Klink finds that neuronal responses increase when off-times increase systematically (from 250 to 2000 ms). This can be explained with neuronal adaptation: when off-durations increase, adaptation levels of neurons have more time to recover to baseline values during blank times and the amount of neuronal activity will be higher.

A recent study by Churchland shows that during constant stimulation longer off-durations will lead to a decrease in neuronal response variability [6]. Using this framework, Klink’s

hypothesis is that longer off-durations will lead to a decrease in neuronal response variability during sequential stimulation. The Fano Factor is a measure for response variability over a full sequence of trials. It is defined as the spike count variance divided by its mean:

$$FF = \frac{\sigma^2}{\mu} \quad (2.1)$$

Churchland shows that stimulus onset reduces the Fano Factor in a variety of cortical areas [6]. To compute the evolving Fano Factor, Klink used a cell-based approach with a 70 ms sliding window in increments of 10 ms across the sequences of stimulus presentations. With this sliding-window-approach, he finds that longer off-durations lead to a decrease in Fano Factors for all three stimuli (figure 2.4).

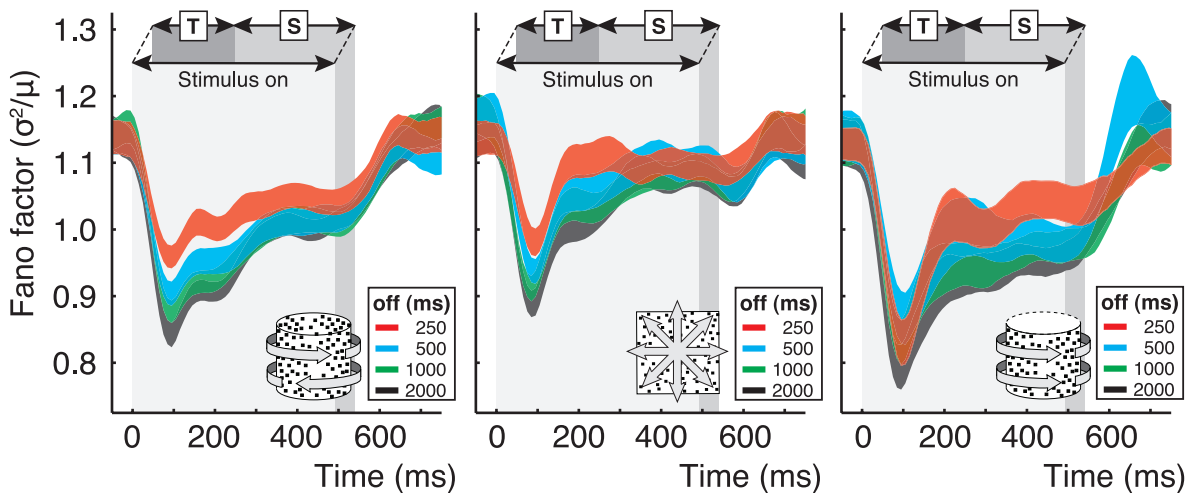


Figure 2.4: Averaged Fano Factors for the three different stimuli (indicated in the panels) and off-durations (the colors) in [17]. Fano Factors were calculated in 10 ms bins aligned to stimulus onset and averaged over the cells. The gray area indicates the moment of stimulus presentation, the transient and sustained phases of the response are marked with [T] and [S] respectively (from [17]).

Klink shows the observed decrease in response variability for longer off-durations is independent of general adaptation effects (local activity contrast-analysis, see [17]). As a third result Klink shows spike-timing patterns become more regular (spike train similarity-analysis, see [17]). An analysis of the local field potential activity suggests this could be due to an increased involvement of the local cortical network. Because the influence of the off-times on the neuronal responses of sensory neurons in area MT is shown for all three stimuli both in the spike-train data as well as the local field potentials, these results suggest a rather general mechanism. Since these neurophysiological experiments are directly connected to earlier human psychophysics and computational work by Noest and Klink in [24, 16], it is an interesting question to see how the neurophysiological results relate to these neurocomputational models.

2.3 Mathematical models

2.3.1 Noest

Noest has developed a phenomenological model for percept-choice sequences during intermittently presented stimuli [24]. Phenomenological rather than biophysical is that neural activity and adaptation are both modeled at a population level. Noest compared the percept-choice dynamics with the dynamics underlying spontaneous switches during constant viewing. As discussed in the introduction, general adaptation effects can account for spontaneous switches since slow adaptation can cause a stable attractor to lose stability and the other attractor to gain dominance. This mechanism is not sufficient to describe the dynamics during sequential stimulation, since the on-off-structure often leads to repetitive structures or more complex mixtures of repetition and alternation.

In order to model percept-switches Noest develops a different approach, by recognizing the on-off-structure forces switches between two different dynamical structures. During blank periods the origin is a stable equilibrium. During stimulation the origin loses stability and two new equilibria emerge, corresponding to the two percepts. Noest formulates a mean-field model that consists of two local fields, corresponding to the membrane voltage components of two separate competing populations. The model is given by the following system of nonlinear differential equations:

$$\tau \frac{\partial H_i}{\partial t} = X_i - (1 + A_i)H_i + \beta A_i - \gamma S[H_j] \quad (2.2)$$

$$\frac{\partial A_i}{\partial t} = -A_i + \alpha S[H_i], i, j \in \{1, 2\}, i \neq j, \quad (2.3)$$

$$S(z) = \begin{cases} \frac{z^2}{1+z^2} & \text{if } z > 0, \\ 0 & \text{if } z < 0. \end{cases} \quad (2.4)$$

with H_i the percept (i)-related component population-activity, X_i the (preprocessed) visual input, A_i the corresponding adaptation levels and S a sigmoidal transformation. As τ is small, membrane voltage dynamics are fast and adaptation dynamics relatively slow. The dynamics underlying percept choices at stimulus onset can be explained by a crucial dependence on differences between adaptation levels at stimuli-onset (see figure 5(a) and 5(b)).

The phenomenological model by Noest can be extended to a more biologically realistic model if pre-rivalry stages are included [16], but the dynamics remain operating on local fields, and as such are difficult to connect and compare with neuronal spike-data from the neurophysiological experiments. Since Noest's model is deterministic and needs an initial 'noisy' push from the symmetrical ideal starting point in order to reproduce percept-sequences, we will now consider neurocomputational models that included noise within their approaches.

2.3.2 Stochastic drift-diffusion model

A stochastic population model for choice-sequences has been developed in [10]. They model two-alternative forced choice task phenomenologically using drift-diffusion models. The model integrates the difference of noisy stimulus information until sufficient evidence for a response is obtained, i.e. a threshold is reached. A decision-making layer receives excitatory input from a sensory layer: this input is either a repetition (R) or an alternation (A) of the stimulus shown

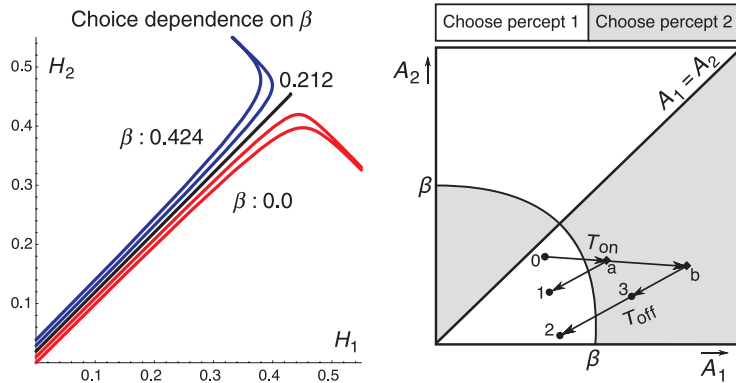


Figure 2.5: a: If the system was in one of the attractors before the most recent interruption, slow adaptation dynamics will lead to asymmetric adaptation levels at the next stimulus onset. If we assume the previous stimulus-presentation attractor 2 was dominant and assuming adaptation is sufficiently slow, we will have $A_1 < A_2$ at the next stimulus onset. This asymmetry changes the dynamics of the system, since the saddle point will shift to the left and the separatrix will move up accordingly (relative to the perfect symmetric case). If the initial point H_i can not be shifted towards the separatrix, the model will always predict alternation. A positive β will create an offset $\beta A_i / (1 + A_i)$ in H_i -levels at stimulus offset and this can compensate the separatrix shift and thus possibly allows repetition. In the figure two different β -trajectories show this crucial dependence on the offset: the red trajectory (percept 1) and the blue trajectory (percept 2) show alternation (from percept 2 to percept 1) and repetition (from percept 2 to percept 2) respectively so repetitions only occur if β is strong enough. The asymmetry in adaptation levels was $A_1 = 0, A_2 = 0.1$ and the black line shows the shifted separatrix. (figure from [24]. **b:** The β -parameter functions as a neural baseline parameter: at stimulus onset (0 in figure) the adaptation value of the corresponding percept will increase: depending on the on-duration and the off-duration alternation and repetition can occur. For relative short on-durations, short off-durations can lead to repetitions (point a to point 1 in figure). For longer on-durations the percept choice depends on the length of the off-duration: short off-durations give alternations (point b to point 3 in figure), whereas sufficiently long off-durations lead to repetitions (point b to point 2 in figure). (figure from [16]).

in the representation before. Since several studies have investigated the crucial influence of the response to stimulus interval (RSI) on choice dynamics, reflected in the choice sequences, biasing mechanisms are introduced to match these observations [26, 5, 15].

A decision is made when a unit reaches a fixed threshold and the evolution of activity-levels of two decision units ($x_1(t), x_2(t)$) are described by stochastic differential equations. The model presents a description of the dynamics during a stimulus representation, given the previous stimulus and including memory bias and rapid decay after responses in the initial conditions. The memory dynamics over trials is as follows, with $S(n - j)$ the stimulus in the $(n - j)$ -th trial:

$$M_R(n) = \alpha_R M_R(n-1) + I_R(n-1) \quad (2.5)$$

$$M_A(n) = \alpha_A M_A(n-1) + I_A(n-1) \quad (2.6)$$

$$I_R(n-1) = \begin{cases} 1 & \text{if } S(n-1) = S(n-2), \\ 0 & \text{otherwise.} \end{cases} \quad (2.7)$$

$$I_A(n-1) = \begin{cases} 0 & \text{if } S(n-1) = S(n-2), \\ 1 & \text{otherwise.} \end{cases} \quad (2.8)$$

They assume biasing strengths $B_{R,n}$ and $B_{A,n}$ in the n -th trial depend linearly on the memory:

$$B_{R,n} = 0.1M_R(n) \quad (2.9)$$

$$B_{A,n} = 0.1M_A(n) \quad (2.10)$$

Finally, they assume biasing strength increases before each trial:

$$b_{R,n}(RSI) = \begin{cases} B_{R,n} \left[1 - e^{-\frac{RSI - T_0}{\tau}} \right] & \text{if } RSI > T_0, \\ 0 & \text{otherwise.} \end{cases} \quad (2.11)$$

Since α_A and α_R are constants between 0 and 1, strength of expectation depends stronger on recent representations. The decision units are coupled by mutual inhibition of strength β through a sigmoidal $f(x_i)$. Each unit has the same time constant τ_c and k is the strength of passive leakage. ρ_i equals $\rho_0 + 0.5$ when stimulus i is shown and $0.5 - \rho_i$ when it is not shown, with $\rho_0 = 0.35$, so this input stimulus functions as an initial bias. The stochastic terms (η_i) are independent and identically distributed Gaussian noise processes. See figure 2.6 for a full schematic description of the modeling approach. The excitatory bias $+B_{i,n}$ is associated with the decision unit that confirms the expectation depending on the memory and an inhibitory bias $-B_{i,n}$ is associated with the decision unit that violates the expectation. So for a previous stimulus 1 expectation of repetition sends positive bias to unit 1 and negative bias to unit 2 and expectation of alternation sends positive bias to unit 2 and negative bias to unit 1. The overall dynamics of the n th trial with expectation-related bias is then:

$$\tau_c \frac{dx_1}{dt} = -kx_1 - \beta f(x_2) + \rho_1 + b_{R,n}(RSI) - b_{A,n}(RSI) + \sigma \eta_1(t) \quad (2.12)$$

$$\tau_c \frac{dx_2}{dt} = -kx_2 - \beta f(x_1) + \rho_2 - b_{R,n}(RSI) + b_{A,n}(RSI) + \sigma \eta_2(t) \quad (2.13)$$

$$(2.14)$$

Similar equations are derived for introducing biases from conflict monitoring, where the conflict monitoring system evaluates conflict and passes this information on to centers responsible for control, triggering them to adjust the strength of their influence on processing, see figure 2.6.

Modeling memory bias, conflict-monitoring bias and post-response bias in the form of initial conditions restrictions, enabled Gao to simulate combinations and test the mechanisms against physiological data. The models output matches psychophysical results and allows

mathematical analysis, but a biophysical interpretation within the context of single neuronal responses is problematic because of the phenomenological nature of the approach. Since there are no straightforward methods to develop a neuronal network model (micro-level) from a population model (macro-level), we consider an approach by Wang and Wong that derived a macro-level model (reduced population models) from the micro-level (detailed neuronal network).

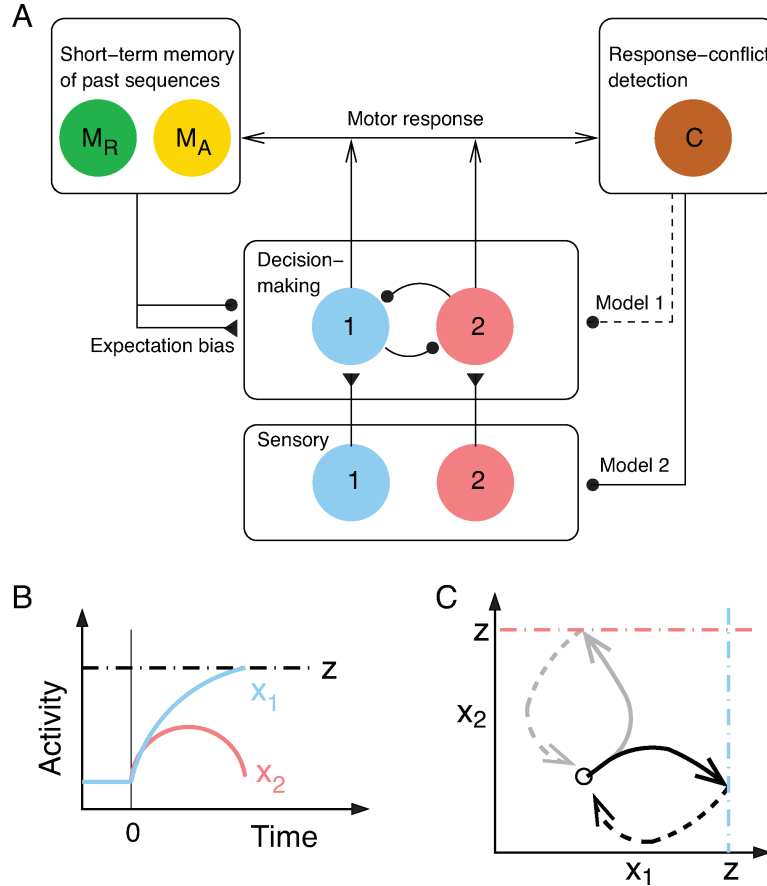


Figure 2.6: Schematic diagram of structure in Gao [10]: filled triangles: excitatory connections, filled circles: inhibitory connections. Two decision units (1) and (2) in the decision layer receive stimulus input from the sensory layer: stimulus (1) excites unit (1) and stimulus (2) excites unit (2), whereas units (1) and (2) are coupled through cross-inhibition. Evidence is accumulated for choices (1) and (2) in the decision layer, receiving an expectation bias that depends on the short-term memory of past trials. These biasing storages of past sequences can excite or inhibit the decision units. Synchronous activity-levels are associated with conflict-monitoring during decision-making and can operate on two levels during subsequent alternations.

2.3.3 Wang and Wong

In [28] Wang and Wong investigate synaptic mechanisms of perceptual decision making by investigating a biophysically realistic cortical network model [27, 4] for a visual discrimination task. They consider LIP-data of monkeys during two-alternative forced-choice visual motion

discrimination tasks [25]. In this task a monkey is trained to indicate the direction of motion in a random dot display with a saccade. Neurons generally show increased persistent activity during a delay period of a few seconds, when the monkey is actively holding the information of the stimulus in its working memory [11]. According to earlier neurophysiological research area LIP is a likely candidate to be a decision-making circuit [25].

The biophysical network (see upper left sub-figure in figure 2.7) consists of leaky integrate-and-fire neurons with AMPA, GABA_A and NMDA receptor-mediated currents. Slow synaptic reverberation is mediated by NMDA receptors and winner-take-all competition is mediated by feedback inhibition from interneurons. Each stimulus activates a small subpopulation of fN_E excitatory cells ($f = 0.15$) and the remaining $(1 - 2f)N_E$ excitatory cells do not respond to stimuli. Neurons receive stochastic Poisson inputs that represent the output from MT cells during stimulation. Strong recurrent excitatory connections within a neural group enable self-sustained persistent activity and slow integration of stimuli leads to dominance of one of the populations and suppression of activity within the other population. The biophysical model is reduced to a two-variable population model in three separate steps, see figure 2.7.

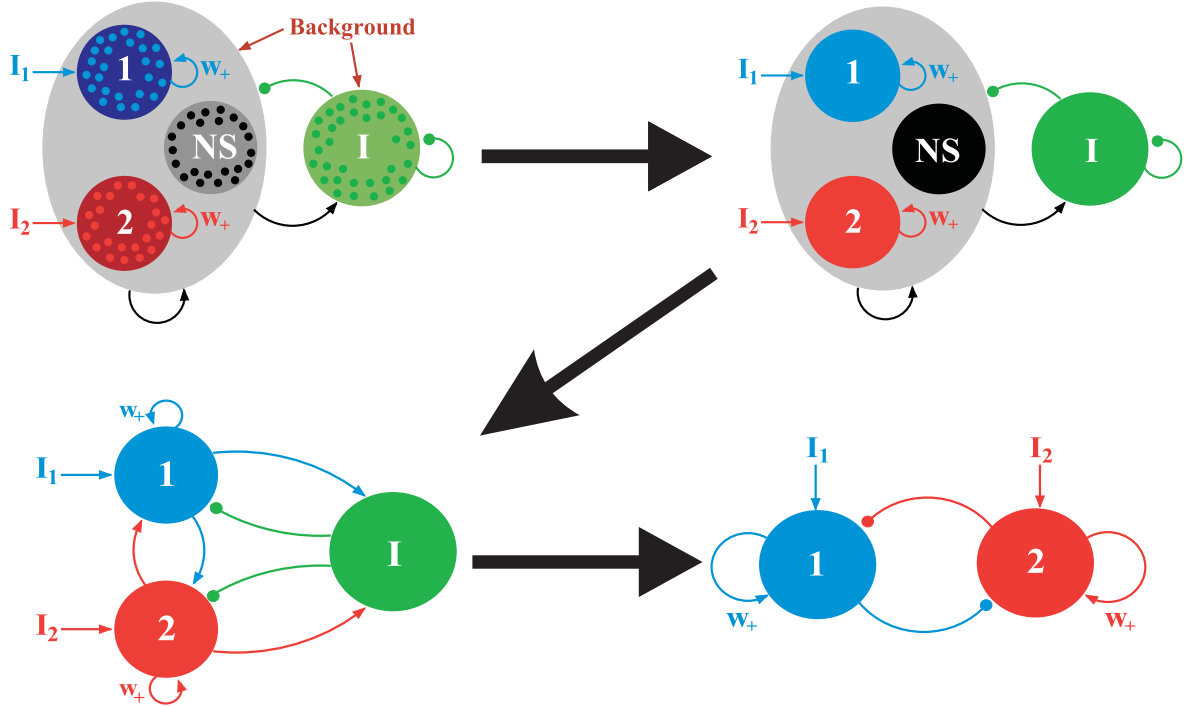


Figure 2.7: Schematic diagram of the structure (size and connectivity) of the initial large network model and the subsequent reductions in [28]. NS: non-selective neurons, I: inhibitory neurons and units 1 and 2 correspond with selective neural populations. Arrows within the figures correspond to excitatory connections; circles correspond to inhibitory connections. The large network receives background inputs (brown arrows) and inputs from external stimulus I_1 and I_2 to the neural populations. A mean-field approach reduces the neuronal network to a system of 11 equations and 4 units (from upper left to upper right). After simplifying the input, linearizing the output of the inhibitory neurons and assuming that non-selective cells are approximately constant the mean-field-system is reduced to a system of 8 equations and 3 units (from upper right to lower left). After assuming that the evolution of the fast variables is much faster than the evolution of the NMDA gating variable, a reduced two-variable model with self-excitation and cross-inhibition is derived (from lower left to lower right).

2.3.4 Laing and Chow

Another spiking neuron model describing the neuronal dynamics during binocular rivalry input was developed by Laing and Chow [18]. The model consists of excitatory and inhibitory conductance-based Hodgkin-Huxley-type neurons. Binocular gratings are modeled as applied current injected at two locations in the network centered around neurons whose preferred orientations differ by 90 degrees, see figure 2.9. Each neuron is tuned to a given orientation (see figure 2.8) and connections between neurons with similar orientation are stronger (Gaussian decay). All cells include a standard transient sodium, potassium and leak current. These are standard Hodgkin-Huxley-type currents, with dynamic gating variables for the potassium and sodium currents. Excitatory neurons receive an afterhyperpolarization current that corresponds with spike frequency adaption and synaptic depression is modeled within the excitatory-to-excitatory connections in synaptic currents, see (2.19), (2.26), (2.20) and (2.27) .

Spike frequency adaptation down-regulates the spiking-activity in the dominant population with a time constant of approximately 80 ms. The afterhyperpolarization is modeled by slow calcium-activated potassium channels. Potassium channels will open up more due to calcium inflow during spikes and consequently, the membrane voltage will become more negative, since potassium's resting potential lies around -80 mV. The equations are based on an approach by McCormick in [23].

Synaptic depression is a form of short-term plasticity within many synapses, which causes a decrease in the amplitude of postsynaptic potentials caused by successive presynaptic spikes. Regarding the modeling and biophysics underlying synaptic depression, Laing and Chow ([18]) refer to Abbott ([1]). Abbott argues that synaptic depression enables postsynaptic neurons to produce equal responses to both slow presynaptic input and to faster presynaptic inputs [1]. The equations were found by fitting the model to experimental findings in slices of rat primary visual cortex [1]. Synaptic depression takes place in the excitatory to excitatory connections with a time constant of approximately 1 second.

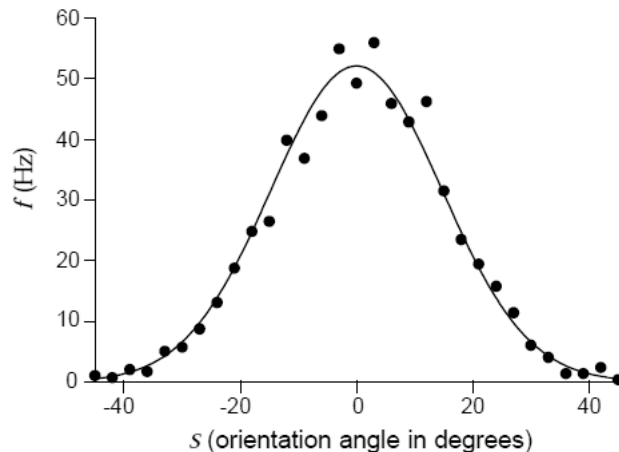


Figure 2.8: Example of a typical tuning curve: average firing rate of a V1 neuron from a cat, plotted as a function of the orientation angle of the light bar stimulus (from [7]).

The equations for the excitatory neurons are:

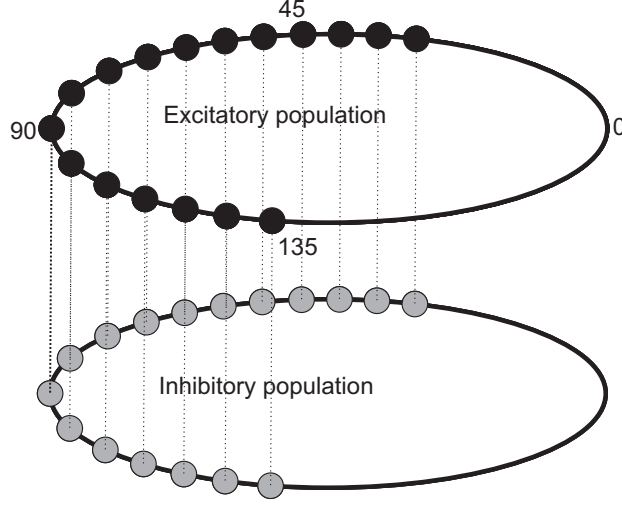


Figure 2.9: Schematic diagram of the applied current in Laing and Chow in [18]. Excitatory neurons (black dots) and inhibitory neurons (grey dots) are coupled and situated on two separate rings. The neurons are labeled with their preferred orientation in degrees. Current is injected to two groups of neurons whose preferred orientations differ by 90 degrees (from [18]).

$$\frac{dV_e}{dt} = I_{\text{syn-exc}} + I_{\text{ext}} - I_{\text{mem}}(V_e, n_e, h_e) - I_{\text{AHP}}(V_e, [\text{Ca}]) \quad (2.15)$$

$$\frac{dn_e}{dt} = \psi [\alpha_n(V_e)(1 - n_e) - \beta_n(V_e)n_e] \quad (2.16)$$

$$\frac{dh_e}{dt} = \psi [\alpha_h(V_e)(1 - h_e) - \beta_h(V_e)h_e] \quad (2.17)$$

$$\tau_e \frac{ds_e}{dt} = A\sigma(V_e)(1 - s_e) - s_e \quad (2.18)$$

$$\frac{d[\text{Ca}]}{dt} = \frac{-0.002g_{\text{Ca}}(V_e - V_{\text{ca}})}{1 + e^{-(V_e+25)/2.5}} - \frac{[\text{Ca}]}{80} \quad (2.19)$$

$$\tau_e \frac{d\phi}{dt} = 1 - \phi - f\sigma(V_e)\phi \quad (2.20)$$

The equations for the inhibitory neurons are:

$$\frac{dV_i}{dt} = I_{\text{syn-inh}} + I_{\text{ext}} - I_{\text{mem}}(V_i, n_i, h_i) \quad (2.21)$$

$$\frac{dn_i}{dt} = \psi [\alpha_n(V_i)(1 - n_i) - \beta_n(V_i)n_i] \quad (2.22)$$

$$\frac{dh_i}{dt} = \psi [\alpha_h(V_i)(1 - h_i) - \beta_h(V_i)h_i] \quad (2.23)$$

$$\tau_i \frac{ds_i}{dt} = A\sigma(V_i)(1 - s_i) - s_i \quad (2.24)$$

The equations for the membrane current I_{mem} , afterhyperpolarization current I_{AHP} , applied current $I_{\text{ext}}(i)$ and synaptic currents $I_{\text{syn-exc}}$ and $I_{\text{syn-inh}}$:

$$I_{\text{mem}}(V_e, n_e, h_e) = g_L(V_e - V_L) + g_K n_e^4 (V_e - V_K) + g_{Na} (m_\infty(V_e))^3 h_e (V_e - V_{Na}) \quad (2.25)$$

$$I_{\text{AHP}}(V_e, [\text{Ca}]) = \frac{g_{\text{AHP}}[\text{Ca}](V_e - V_K)}{([\text{Ca}] + 1)} \quad (2.26)$$

$$I_{\text{ext}}(i) = \frac{0.4}{\sqrt{2}} \left[e^{-\frac{20(i-N/4)^2}{N}} + e^{-\frac{20(i-3N/4)^2}{N}} \right] - 0.01 \quad (2.27)$$

$$I_{\text{syn-exc}}^j = \frac{1}{N} (V_{ee} - V_e^j) \sum_{k=1}^N g_{ee}^{jk} s_e^k \phi^k + \frac{1}{N} (V_{ie} - V_e^j) \sum_{k=1}^N g_{ie}^{jk} s_i^k \quad (2.28)$$

$$I_{\text{syn-inh}}^j = \frac{1}{N} (V_{ei} - V_i^j) \sum_{k=1}^N g_{ei}^{jk} s_e^k + \frac{1}{N} (V_{ii} - V_i^j) \sum_{k=1}^N g_{ii}^{jk} s_i^k \quad (2.29)$$

For the remaining functions, constants and parameter-values, we refer to the appendix.

Laing and Chow convert their neuronal network into a network of rate neurons. They first derive the equations for the slow processes, since they are slower and both driven by the post-synaptic activity. A leaky integrator describes the overall mechanism of spike frequency adaptation: if a neuron becomes more active, its adaptation-variable will increase which in return will decrease the activity of the neuron. With a_i as the generalized adaptation variable of neuron i and $A_i(t)$ as the instantaneous firing rate of neuron i , they find:

$$\frac{da_i}{dt} = -\frac{a_i}{\tau_a} + A_i(t) \quad (2.30)$$

By assuming that neuronal activity is driven by synaptic inputs through a gain function f , with w_{ij} as the synaptic weights, $U_j(t)$ as the postsynaptic response of neuron j and I_i as the external input to neuron i , they find:

$$A_i(t) = f \left(\sum w_{ij} U_j(t) - a_i + I_i \right) \quad (2.31)$$

Equation (2.31) is substituted in equation (2.30) in order to obtain:

$$\frac{da_i}{dt} = -\frac{a_i}{\tau_a} + f \left(\sum w_{ij} U_j(t) - a_i + I_i \right) \quad (2.32)$$

An expression for synaptic depression is derived analogously, with g_i the generalized depression variable of neuron i :

$$\frac{dg_i}{dt} = -\frac{g_i}{\tau_g} + f \left(\sum w_{ij} U_j(t) - a_i + I_i \right) \quad (2.33)$$

In line with an approach by Ermentrout [8], postsynaptic responses are modeled as the integral over all postsynaptic activity multiplied by a linear filter function $\epsilon(t)$:

$$U_j(t) = \int_{-\infty}^t \epsilon(t-s) A_j(s) ds \quad (2.34)$$

By assuming $\epsilon(t) = e^{-t}$ a differential equation for $U_j(t)$ is derived:

$$\frac{dU_j(t)}{dt} = \frac{d}{dt} \left(\left[-e^{-(t-s)} A_j(s) \right]_{-\infty}^t \right) \quad (2.35)$$

$$= f \left(\sum w_{ij} U_j(t) - a_i + I_i \right) \quad (2.36)$$

Equations (2.32), (2.33) and (2.36) describe the evolutions of rate neurons.

Since excitation dominates inhibition within the dominant population during the dominance duration and inhibition in the other population dominates excitation, it is sufficient to model binocular rivalry switches on a population level by considering the dynamics of two mean-field populations with self-excitation and cross-inhibition. The overall network dynamics can be approximated by considering spatially averaged variables for activity, adaptation and depression for two populations. By including noise and using the rate equations versions of equations (2.32) and (2.33), they derive a system of 6 mean-field differential equations for the two populations:

$$\frac{du_1}{dt} = -u_1 + f(\alpha u_1 g_1 - \beta u_2 g_2 - a_1 + I_1) \quad (2.37)$$

$$\frac{du_2}{dt} = -u_2 + f(\alpha u_2 g_2 - \beta u_1 g_1 - a_2 + I_2) \quad (2.38)$$

$$\tau_a \frac{da_1}{dt} = -a_1 + \phi_a f(\alpha u_1 g_1 - \beta u_2 g_2 - a_1 + I_1) \quad (2.39)$$

$$\tau_a \frac{da_2}{dt} = -a_2 + \phi_a f(\alpha u_2 g_2 - \beta u_1 g_1 - a_2 + I_2) \quad (2.40)$$

$$\tau_d \frac{dg_1}{dt} = 1 - g_1 - g_1 \phi_d f(\alpha u_1 g_1 - \beta u_2 g_2 - a_1 + I_1) \quad (2.41)$$

$$\tau_d \frac{dg_2}{dt} = 1 - g_2 - g_2 \phi_d f(\alpha u_2 g_2 - \beta u_1 g_1 - a_2 + I_2) \quad (2.42)$$

This reduced model allows a slow-fast analysis because of the different and separate timescales, and is eventually used to derive an exact expression for the distribution of dominance durations observed during human psychophysical experiments. Although the overall modeling-structure is different from our approach by focusing on the dependence of the interstimulus interval t_{off} on sequential effects in perceptual choices, this model does provide a useful starting point on both the micro-level as the macro-level.

The neuronal network models by Laing and Chow [18] and Wang and Wong [27] are the main candidates as starting points for the extension towards interrupted sequences of stimuli, because neuronal networks provide the desired neuronal structure and reproduce psychophysical results. We take Laing and Chow as a starting point, because their set-up is remarkably simpler and smaller when compared with the detailed structure of thousands of neurons in Wang and Wong [27]. The population approaches by Laing and Chow [18], Noest [24], Wang and Wong [28] and Gao [10] can be used to compare our reduced description of the neuronal network model.

3 Methods

In this section we will describe our overall modeling approach: we start with the original Laing and Chow model and validate the model by reproducing their results. We then include interrupted sequences of stimuli and investigate the influence of several parameters on the models behavior, such as the on-durations and off-durations of the applied current. We will show the choice-sequences resulting from the interrupted version of the Laing and Chow model connect well with the psychophysical data from Klink and Noest [16], [24].

3.1 Simulating the model

The spiking-neuron network by Laing and Chow consists of two coupled sets of neurons: excitatory and inhibitory neurons. An excitatory neuron is described by 6 differential equations and an inhibitory neuron by 4 differential equations and neurons are synaptically connected. We take 60 excitatory and 60 inhibitory neurons and use a forward Euler scheme to approximate the $10 \times N$ -dimensional system. Given Matlab's restrictions on simulating large sets of differential equations over time, this is advantageous because a forward Euler scheme is rather fast when compared to build-in solvers. In a forward Euler scheme approximations of the values at time level $j + 1$ are determined by the values of the approximate solution at the time level j . Hence, the initial condition together with the chosen time-step and neuronal configuration completely determine the approximation of the entire evolution of the state-variables. So, because the Euler scheme uses a fixed time step, the entire solution matrix can be preallocated at forehand, which is computationally efficient.

Laing and Chow use a time-step of 0.02 ms, although similar time-steps give similar results. As initial conditions we take:

- Resting potential excitatory and inhibitory neurons: -60 mV
- Gating variables (n_e, h_e, n_i, h_i) : randomly initialized between 0 and 1
- Initial state of synaptic coupling vectors is such that the first 30 neurons are initially 0.2 and the last 30 neurons are initially 0: this difference in synaptic coupling will lead to the left percept (corresponding with the first 30 neurons) becoming dominant at $t = 0$
- Calcium concentration for all neurons: 0 (no initial calcium active within the network)
- Initial synaptic depression variable: 1 (no initial synaptic depression applying on the network)

3.2 Output measures

Simulating with the Euler scheme allows us to monitor all state-variables over time. We can use these evolutions to obtain a full picture of the governing dynamics, and investigate the underlying patterns at the neuronal and population level. Of particular interest is the evolution of the membrane voltage of single neurons, see figure 3.1

Since we are interested in the spiking activity of the entire network, we use the computed evolutions to construct a spike rastergram. We say that neuron i fired if the potential V_i was above a threshold of 20 mV. This happens during short intervals and we take the time of the action potential to be the time of the maximal potential. Note that within our preallocation

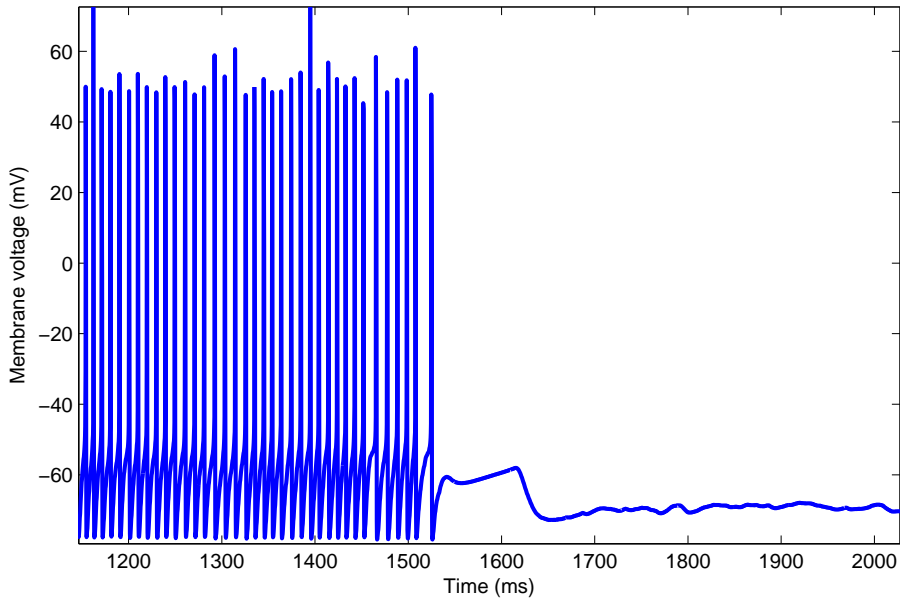


Figure 3.1: Membrane voltage neuron 15 from the excitatory population. This neuron corresponds to one of the sites at which current is injected and as such can be understood as the center of the right (left) population within the excitatory population, whereas neuron 45 would be the left (right) center. After a period of repeated spiking the membrane potential returns to resting state around -65 mV, the interspikeinterval is approximately 10 ms during these sequences of action potentials. Parameter settings are similar to [18] and can be found in the appendix. The value of f varies between 0.5 and 1.5 in [18] and crucially influences the length of dominance durations. In these simulations we used $f = 0.9$.

set-up, the evolutions are down-sampled over time, however, this is still a reasonable approximation. All the spike times make up the spike rastergram, typical examples are shown in figure 3.2 for the excitatory and the inhibitory rastergrams. It turns out that it is enough to consider only the excitatory-rastergram, because the activity within the inhibitory population shows the same dynamics but activity is generally more spread-out over the entire population, making it harder to distinguish boundaries between populations. The typical patterns that we observe is that of activity bumps around neuron 15 and neuron 45. These neurons are situated at 1/4th and 3/4th of the population and correspond to the sites within the population that receive maximal input, compared to the other inputs. Activity is centralized around one of the foci and is alternating between the two focuses. If we think of activity around a focus as corresponding to perceiving one of the two percepts, activity-bumps within the model suggest switches on a perceptual level as in binocular rivalry.

Since the experimental data we consider [16], [17] was analyzed using peri-stimulus time histograms (PSTH), we construct this measure as well to evaluate our spike data.

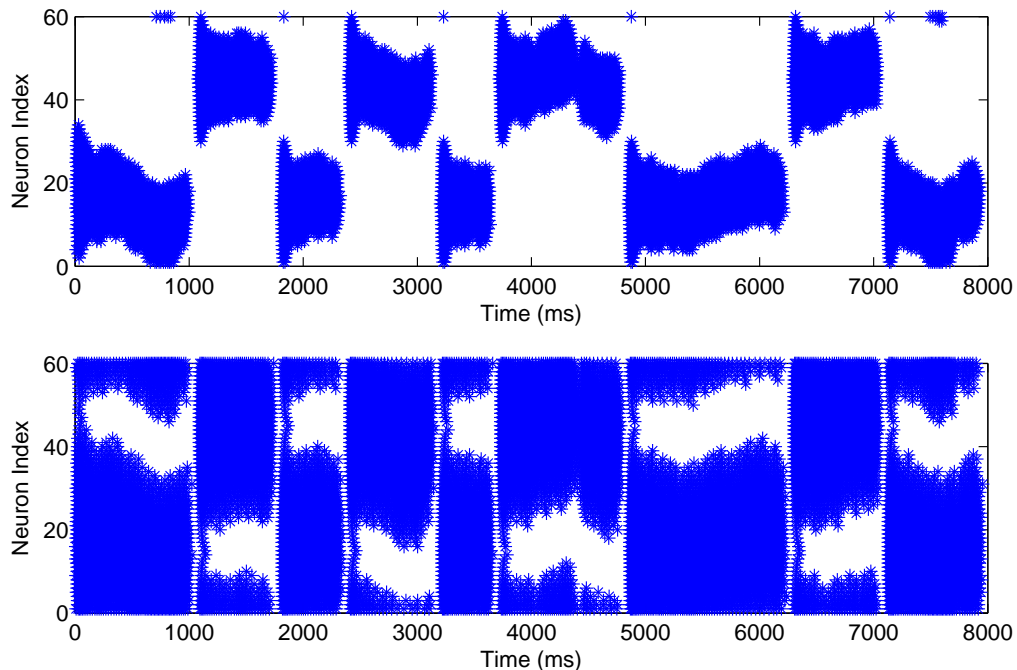


Figure 3.2: Spike rastergrams for the excitatory population (top) and inhibitory population (below), with $f = 0.9$). The dynamical structure within both populations is similar, although the inhibitory activity is more spread out through the population. Spike frequency adaptation and synaptic depression only acting upon the excitatory population might be a possible explanation for this, although it should be noted the model’s dynamics is highly sensitive to the synaptic coupling parameters. Activity patterns are focused around neuron 15 and neuron 45, corresponding to the (1/4)th neuron of the population and the (3/4)th of the population respectively if neurons are situated on a ring. Activity patterns switch back and forth between the two subpopulations, revealing a competition between the two. The time a subpopulation remains dominant, the dominance duration, varies roughly between 800 ms and 1500 ms.

3.3 Validation

Laing and Chow validated their model by testing it against well-established psychophysical results within the domain of binocular rivalry. Because these results matched sufficiently, their model can be qualified as biophysically realistic. In order to check whether our code is adequate, we test simulated results against the established results in Laing and Chow. This way, our results will be in line with the psychophysical outcomes too. This step is especially important because we want to elaborate the model by Laing and Chow to describe the dataset by Klink, which has its own very specific experimental criteria that the model should meet.

3.3.1 Distribution of dominance duration

The time a population remains dominant around one of the two sites is called the dominance duration. The dominance duration within a spike rastergram is closely associated with the

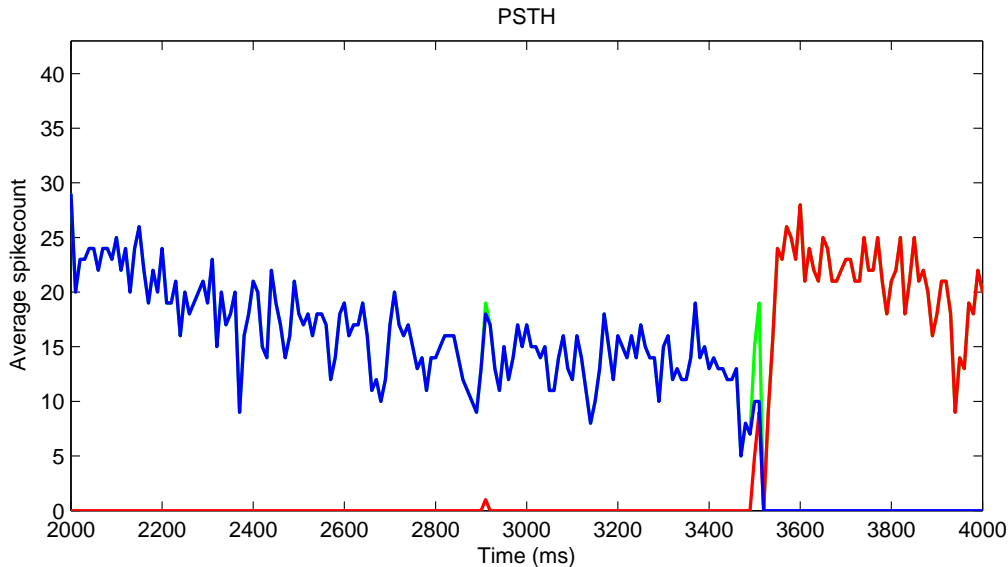


Figure 3.3: PSTH of the activity of the excitatory population. Blue line: evolution of the average firing rate of neuron 1,...,30. Red line: evolution of the average firing rate of neuron 31,...,60. Green line: evolution of the average firing rate of the entire excitatory population, and as such the green line is the sum of the blue line and the red line. At the beginning of the time-interval the blue population is dominant, but around 3500 a switch occurs and the red population gains dominance while the blue population becomes approximately silent. Average firing rates were computed with a time bin of 10 ms and $f = 1.1$.

duration the corresponding percept is dominant. As can be seen in a rastergram (figure 3.2) these durations seem to be irregular. Given the spike times of all the neurons during a simulation, we typically see burst-like behavior within a spiking-array. We compute the distribution of dominance durations by comparing the calcium evolution of the two center-neurons that directly receive current (neuron 15 and neuron 45) and define their intersections as percept-switch times, see figure 3.4.

3.3.2 Largest Lyapunov exponent

Laing and Chow explain the established distribution of the dominance durations and irregularity of subsequent durations by determining the value of the largest Lyapunov exponent. The system of simulated differential equations is completely deterministic, after the initial conditions have been initialized. Yet, we have seen dominance distribution have a specific distribution and it has been shown that subsequent dominance durations are uncorrelated [18]. They relate both observations with the largest Lyapunov exponent, which indicates whether a dynamical system being chaotic. It is a measure for the rate of separation of infinitesimally close initial trajectories. If the exponent is positive, it suggests neighboring trajectories separate exponentially fast, hence, that the system is chaotic. We estimate a positive largest Lyapunov exponent as well, indicating the system is also chaotic, see figure 3.5.

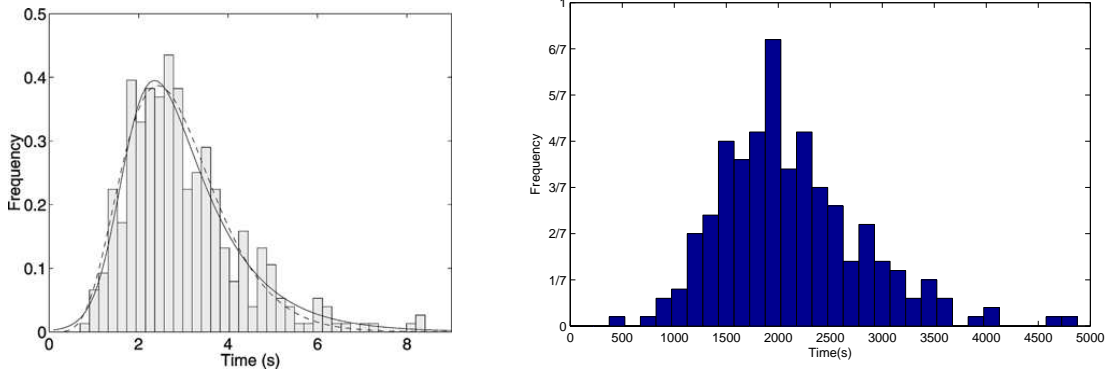


Figure 3.4: Comparison of distribution of dominance durations between [18] and our simulations: (a) distribution of dominance durations by Laing and Chow from [18] (b) our results with a time-duration of 500 seconds and $f = 0.5$. Since the exact parameter settings during their experiments are not specified in [18], reproducing their result is rather difficult. The value of f has a crucial influence on the length of the dominance durations and the overall simulation-time might influence the distribution. In addition, Laing and Chow do not indicate how they determine their durations: the spiking data, the calcium-evolution or the phi-evolution might all be used and it is unknown to what extent the choice of the variable influences the exact configuration of the distribution. Despite the differences in duration lengths, the overall shape of the curves are very similar. Both distributions are unimodal and skewed and have a long tail for longer durations. We conclude our dominance duration distribution provides a satisfactory connection with the results from Laing and Chow.

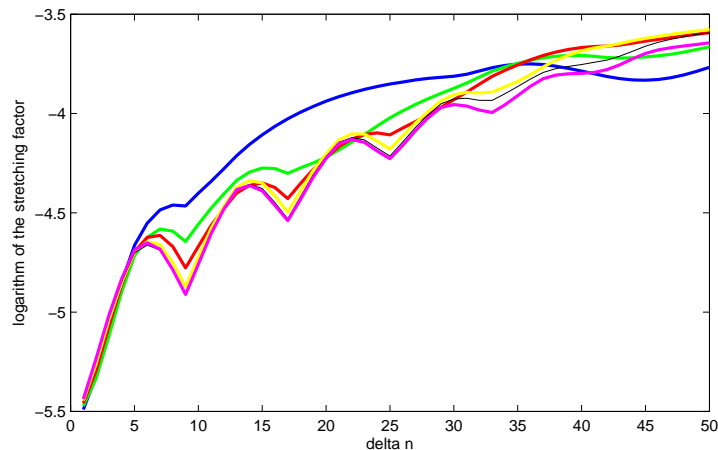


Figure 3.5: Estimation of the maximal Lyapunov exponent of the simulated calcium-data during spontaneous switches. Laing and Chow find 40 s^{-1} as the largest Lyapunov exponent, we estimate 0.05 s^{-1} . Maximal Lyapunov exponents were computed with the algorithm lyap_k from software environment Tisean, available http://www.mpipks-dresden.mpg.de/~tisean/TISEAN_2.1/index.html. This algorithm makes use of an algorithm by Kantz in [13]. The rather big difference in estimates might be due to the fact that Laing and Chow did not specify how they computed their estimate and estimating largest Lyapunov exponents is often a delicate procedure. However, since both estimates are positive, they indicate deterministic chaos and this is sufficient for our approach.

3.3.3 Second Level's proposition

Another aspect of binocular rivalry is that if the strength of the stimulus to one of the eyes is changed, this affects the mean dominance duration of the unchanged eye, not the mean dominance duration of the eye whose stimulus strength was changed. That is, decreasing the strength of the stimulus to eye 1 leads to a nonlinear increase in the mean dominance duration of eye 2 and a small decrease in the mean dominance duration of eye 1. In order to test this hypothesis the equation for the applied current needs to be adjusted by introducing a contrast-parameter ψ for one of the Gaussians, see figure 3.6.

$$I_{\text{ext}}(i) = \frac{0.4}{\sqrt{2}} \left[e^{-\frac{20(i-N/4)^2}{N}} \right] + \frac{\psi}{\sqrt{2}} \left[e^{-\frac{20(i-3N/4)^2}{N}} \right] - 0.01 \quad (3.1)$$

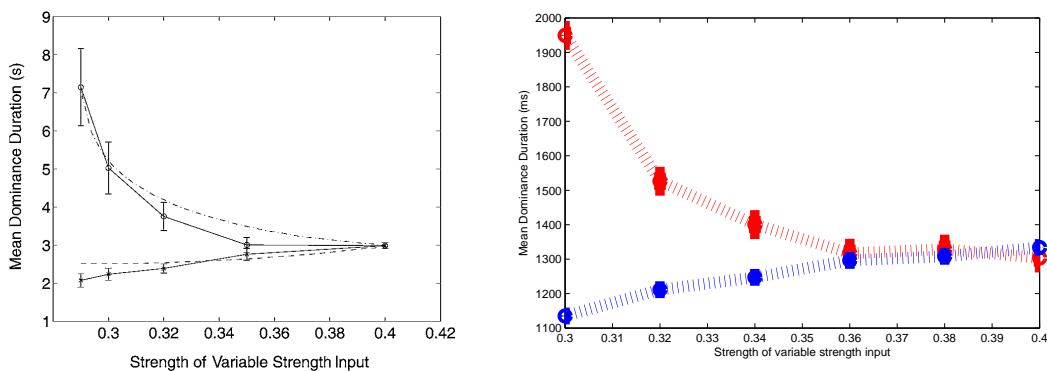


Figure 3.6: Comparison of second Levelt proposition between [18] and our simulations: (a) results by Laing and Chow [18] (b) our results with a time-duration of 100 seconds and $f = 0.7$. Since the exact parameter settings during their experiments are not specified in [18], reproducing their result is rather difficult, as in figure 3.4. Dominance durations were determined by looking at the evolution of the calcium-concentration, which we found is a stable indicator of dominance of a subpopulation. Despite the differences in mean dominance durations, the overall shape of the curves are very similar, showing the mean dominance duration of the subpopulation with unchanged strength increases, while the mean dominance duration of the subpopulation with decreased strength remains approximately constant.

In conclusion, we are able to reproduce results on the distribution of the dominance durations, the largest Lyapunov exponents and the second Levelt proposition and this leads us to believe our model functions similarly to theirs. Simulations and comparison with the original code (C.R. Laing, personal communication) confirmed this conclusion. Given our basic Laing and Chow framework, we can now extend the model with the on-off-structure.

3.4 On-off-structure

In order to connect our model with the approaches by Noest and Klink, we need to enable stimulation with sequences of on-off-cycles instead of only constant stimulation [17], [16], [24]. To implement a sequence of interrupted stimulus-presentations with a fixed on-duration and off-duration, the constant stimulus I_{ext} is multiplied with a periodic block-pulse $y(t)$. Mathematically $y(t) = \left(\frac{1}{1+e^{-y_1(t) \cdot k}} \right) \cdot \left(1 - \frac{1}{1+e^{-y_2(t) \cdot k}} \right)$ where $y_1 = \sin\left(\frac{2\pi t}{t_{\text{on}}+t_{\text{off}}}\right)$ and $y_2 = \sin\left(\frac{2\pi(t+t_{\text{on}})}{t_{\text{on}}+t_{\text{off}}}\right)$

and k a large positive integer. The resulting periodic stimulus consists of a repeated sequence of on-off-cycles with on-duration t_{on} and off-duration t_{off} , see figure 3.7.

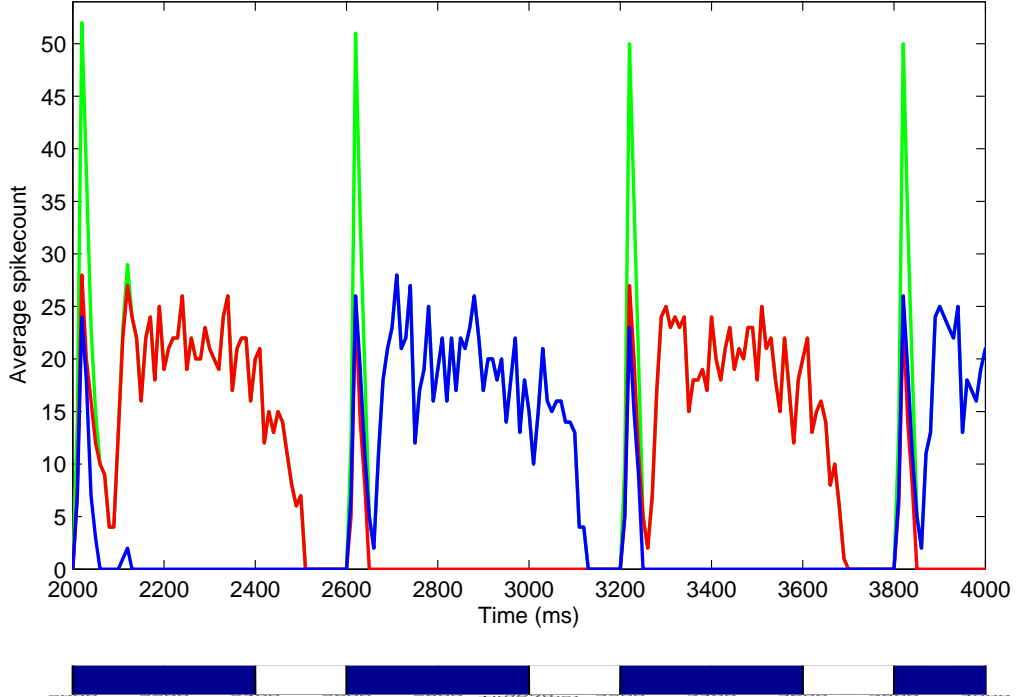


Figure 3.7: PSTH during new stimulation-paradigm with on-off-structure. (a) PSTH of the activity of the excitatory population during stimulation with on- and off-duration (b) block pulse indicating stimulus onset and stimulus offset. Blue line: evolution of the average firing rate of neuron 1,...,30. Red line: evolution of the average firing rate of neuron 31,...,60. Green line: evolution of the average firing rate of the entire excitatory population, and as such the green line is the sum of the blue line and the red line. Average firing rates were computed with a time bin of 10 ms and $f = 1.1$, $t_{\text{on}} = 400$, $t_{\text{off}} = 200$. From the PSTH we can conclude these settings lead to alternations.

In order to connect the new model approach to the human psychophysics results, a close examination of the behavior of the network within the new structure is essential. The new on-off-structure might crucially influence the underlying dynamics of the networks behavior. Laing and Chow discuss the overall network-behavior in relation under constant stimulus conditions with their reduced model [18]. They show that depending on the parameter-settings, the models behavior can be in either an all-on-state (synchronous activity through the entire population), the off-state (no activity at all) and switch-rivalry-state. We expect these states to be within the dynamical behavior of the interrupted model, but we need to take into account the possibility that the interrupted structure might also lead to new patterns of behaviors.

4 Results

Since the dynamical structure of the on-off-paradigm is different than the constant-stimulation-paradigm, different types of activity emerged in the new on-off-paradigm. We initially set the on-duration T_{on} to 500 ms and hypothesized that we should find alternations when the off-duration T_{off} lies in the range from 125 to 500 ms and repetitions within the range from 875 to 1250 ms. Since the effective amount of applied current is less than the effective amount of applied current during constant stimulation, we considered changing the width and amplitude of the applied current as possible control-parameters to force the behavior of the on-off-model to generate the desired activity patterns at onset and offset of the stimuli.

By structurally varying the amplitude and width, we categorized the types of behavior that emerge within the new stimulation-paradigm: an all-on-state, an all-off-state, a binocular-rivalry state, patterns of irregular activity, short volleys of simultaneous activity and traveling waves, see figure 4.1. States with continuous forms of activity during an on-off-cycle, such as patterns of traveling waves or the all-on, do not match with the psychophysical set-up during the experiments in [16, 24], since during the off-duration no stimuli is shown and cannot be perceived. Small periods of initial synchronous activity at stimulus-onset ("volleys") might correspond to perception of a blurred mixture.

Binocular rivalry-switching behavior was found for applied current with a width of 40 and an amplitude of 0.2. This suggests that in order to avoid unwanted behavior such as all-off states or waves, the applied current should have a moderate amplitude and a relatively large width. In this case, one of the two populations becomes dominant right after stimulus-onset and remains dominant until the end of the on-duration. At the start of the off-duration, both populations almost immediately become inactive and will remain silent until the next stimulus-onset, where the entire pattern will start repeating itself.

4.1 Off-durations

Varying the durations of the off-periods while keeping the on-duration fixed, allows to categorize the behavioral patterns that emerge for different off-durations. We set $t_{\text{on}} = 500$ ms and varied t_{off} between 125 ms and 1500 ms with increments of 125 ms. The model was simulated for at least 50 seconds to give a reliable estimation of the overall behavioral patterns, with $f = 1.1$, $g_{\text{AHP}} = 0.055$ (slightly higher than the original 0.05 in [18]) and with amplitude 0.2 and width 40 for the applied current.

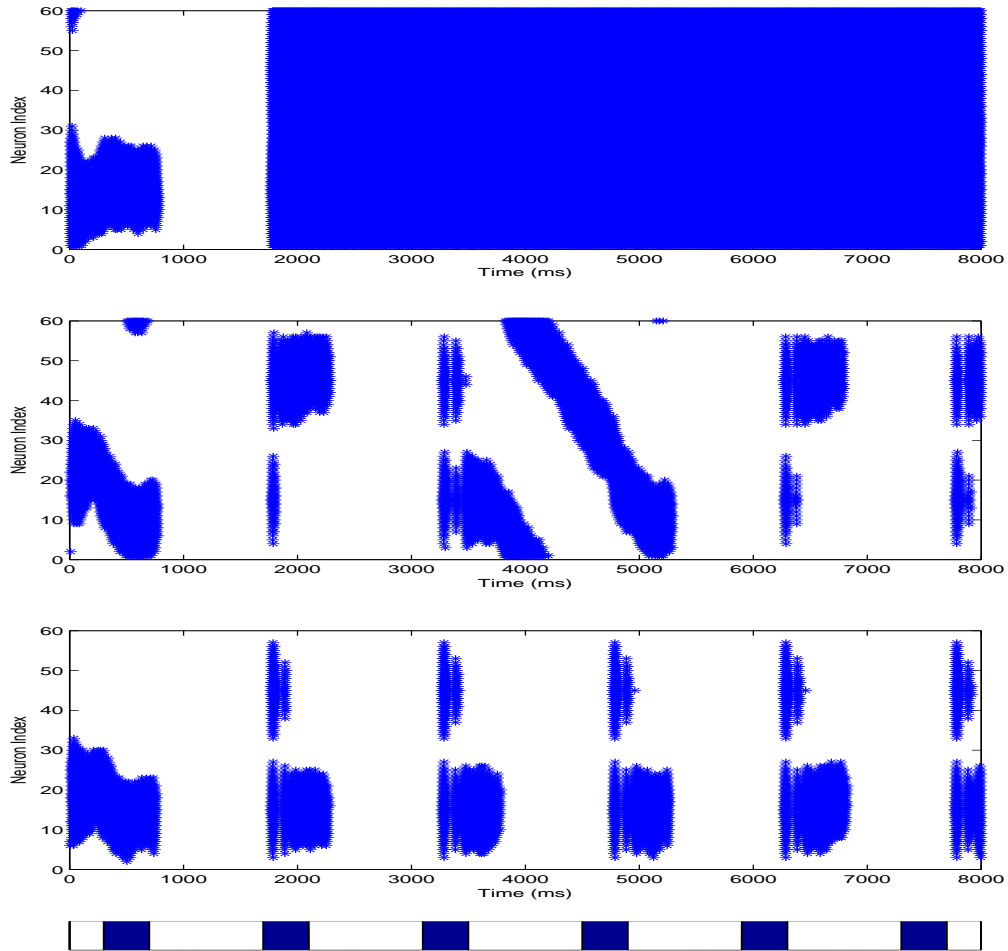


Figure 4.1: Different types of response patterns with $t_{\text{on}} = 500$ and $t_{\text{off}} = 500$. (a): All-on-state activity (width = 10) (b): waves and volleys (width = 40) (c): normal rivalry with a small amount of synchronous activity at stimuli-onset (width = 20).

Off-duration	Behavior	Volleys
125	Alternation	No
250	Alternation	No
375	Alternation	Yes
500	Alternation	No
625	Alternation	No
750	Alternation/repetition	no
875	Alternation/repetition	No
1000	Repetition/alternation	Yes
1125	Repetition/alternation	Yes
1250	Repetition	Yes
1375	Repetition/alternation	Yes
1500	Repetition/alternation	Yes
5000	All-on	-
10000	All-on	-

We computed the percentage of percept repetition during simulations and compared this with figure 4 in [24] by Noest. In the low off-duration range, results are similar although it should be noted we did not take volleys and other types of irregular types of activity in account and as such, the percentage of repetitions is only a percentage of the normal activity during the simulations. When off-durations increase, repetitions percentage increase as well and in the range of 1000 ms and 1250 ms mainly only repetitive patterns occur. If the off-duration is increased even more, we find repetition percentage decrease again. This indicates the mechanisms responsible for inducing repetitions has a timescale of approximately 1250 ms.

Off-duration	On-duration: 500 ms	On-duration: 750 ms
250	10%	5%
500	10%	5%
750	40%	10%
1000	90%	80%
1250	100%	100%
1500	80%	90%

We also found mixtures of alternations and repetitions, where a number of repetitions occurred before an alternation, or a number of alternations before a repetition (see figure 4.2). These more complicated structures are also found in the work by Klink en Noest [24], [16]. In order to investigate the dynamical differences between the different types of behavior, we examined the evolution of the slow variables (figure 4.3 and figure 4.4). This is in line with Noest's general explanation of percept-sequences at stimulus onset due to differences in adaptation-levels [24] and Laing and Chow's observation that adaptation and synaptic depression are both needed to generate switches in the network [18].

4.1.1 Alternation

Figure 4.3 shows the evolution of the calcium-concentration and the synaptic variable of two single excitatory neurons, one neuron from the left population and one neuron from the right population with $t_{\text{on}} = 500, t_{\text{off}} = 250$ ms. In the evolutions of the slow variables we found that the same-switching process occurs as observed in the spike rastergrams. In this case, one of the two populations becomes dominant right after stimulus-onset and remains dominant until the end of the on-duration. As the off-duration starts, both populations immediately drop their activities and will remain silent until the next stimulus-onset. At this stimulus-onset, the population that was suppressed in the previous cycle becomes dominant.

4.1.2 Repetition

In the case of repetition, one of the two populations always dominates the activity and this is reflected in the dynamical evolutions of the slow processes within the two neurons, see figure 4.4 with $t_{\text{on}} = 500, t_{\text{off}} = 1250$ ms. In this case, one of the two populations becomes dominant right after stimulus-onset and remains dominant until the end of the on-duration. As the off-duration starts, both populations immediately drop their activities and will remain silent until the next stimulus-onset and at every stimulus-onset the same population will gain dominance.

Figures 4.4 and 4.3 show the results from the neuronal network model with on-off-structure are very similar to the human psychophysics results found by Klink and Noest in

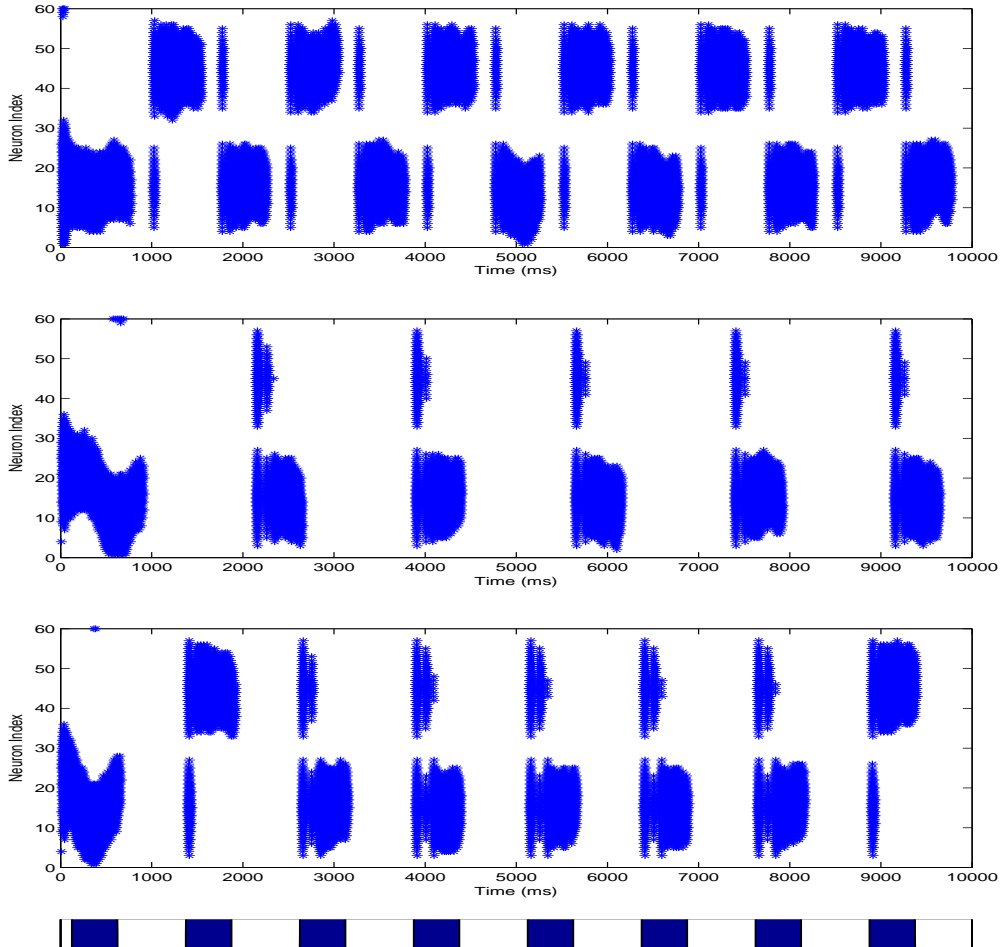


Figure 4.2: Spike rastergrams showing alternation, repetition and mixtures of alternation and repetition within their choice-sequences (a): alternation with $t_{\text{on}} = 500$, $t_{\text{off}} = 250$, (b) repetition with $t_{\text{on}} = 500$, $t_{\text{off}} = 250$ and (c) repetition with $t_{\text{on}} = 500$, $t_{\text{off}} = 750$. In all simulations $f = 1.1$, $g_{\text{AHP}} = 0.055$ and applied current with amplitude 0.2 and width 40.

[16, 24]. There is a clear connection between the micro-level of these neuronal responses during the on-off-structure and the macro-level of human psychophysics percept-sequences during on-off-structure. Since Noest and Klink describe the psychophysics data with a phenomenological model, we considered reduced approaches of our network model. This allows comparison between the approaches by Noest and Klink, but since our model starts from a biophysical realistic starting point, a reduced description might provide insight in the underlying mechanisms governing the dynamics of percept-choice at stimulus-onset. This insight might then be used to eliminate unwanted activity-patterns such as volleys and waves.

4.2 Slow processes

Laing and Chow note that spike rate frequency adaptation and synaptic depression are both needed to generate spontaneous switches. Since we are only interested in the dynamics at stimulus onset and not the spontaneous switches - in fact spontaneous switches typically never

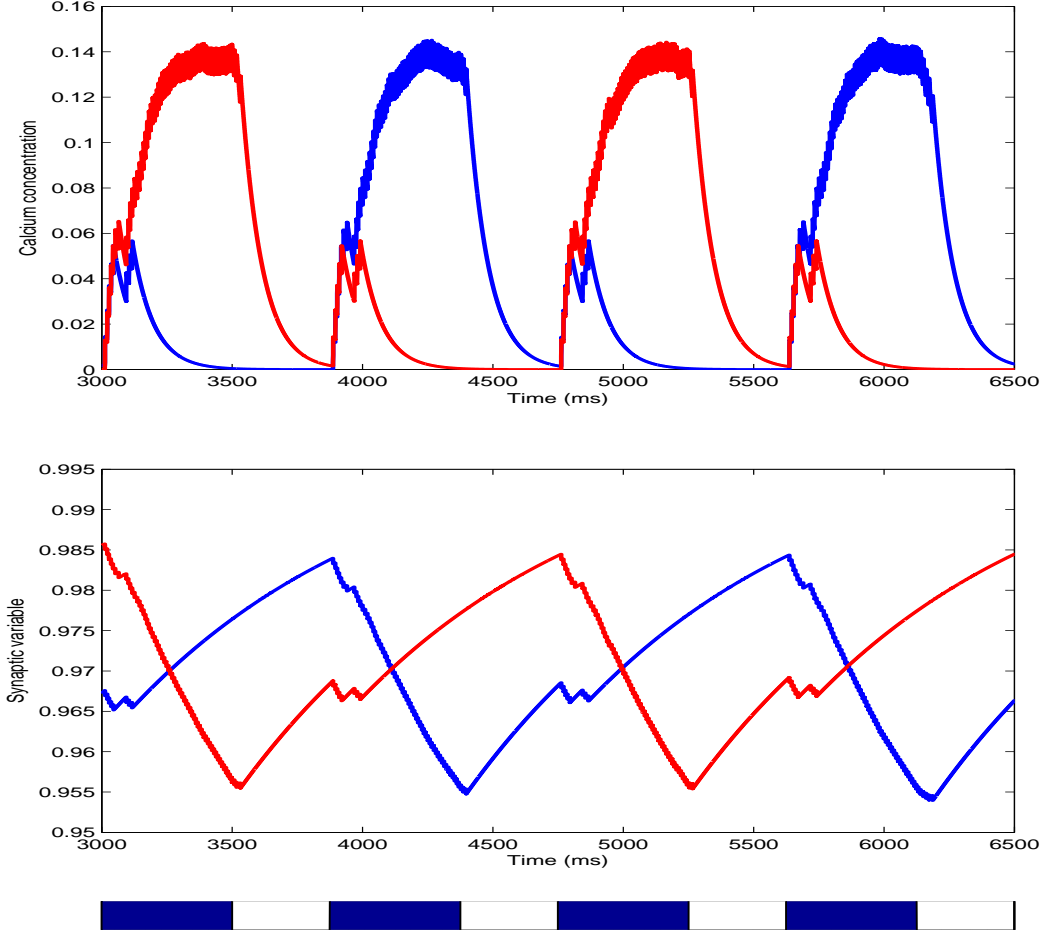


Figure 4.3: Slow variables evolutions for two single neurons during one cycle in the alternation-state. $t_{\text{on}} = 500$, $t_{\text{off}} = 250$. Blue lines correspond to an excitatory neuron from the left population, red lines correspond to an excitatory neuron from the right population. (a): calcium evolution, (b) evolution of synaptic variable.

occur during the on-off-structure, because the on-duration is relatively short - the question arises whether both slow processes needed in order to obtain the repetition and alternation structure during on-off-cycles. In line with Noest in [24] we first considered the reduced model with only spike-frequency adaptation:

$$\frac{du_1}{dt} = -u_1 + f(\alpha u_1 - \beta u_2 - a_1 + I_1) \quad (4.1)$$

$$\frac{du_2}{dt} = -u_2 + f(\alpha u_2 - \beta u_1 - a_2 + I_2) \quad (4.2)$$

$$\tau_a \frac{da_1}{dt} = -a_1 + \phi_a f(\alpha u_1 - \beta u_2 - a_1 + I_1) \quad (4.3)$$

$$\tau_a \frac{da_2}{dt} = -a_2 + \phi_a f(\alpha u_2 - \beta u_1 - a_2 + I_2) \quad (4.4)$$

Laing and Chow showed this reduced model can lead to four different types of behavior:

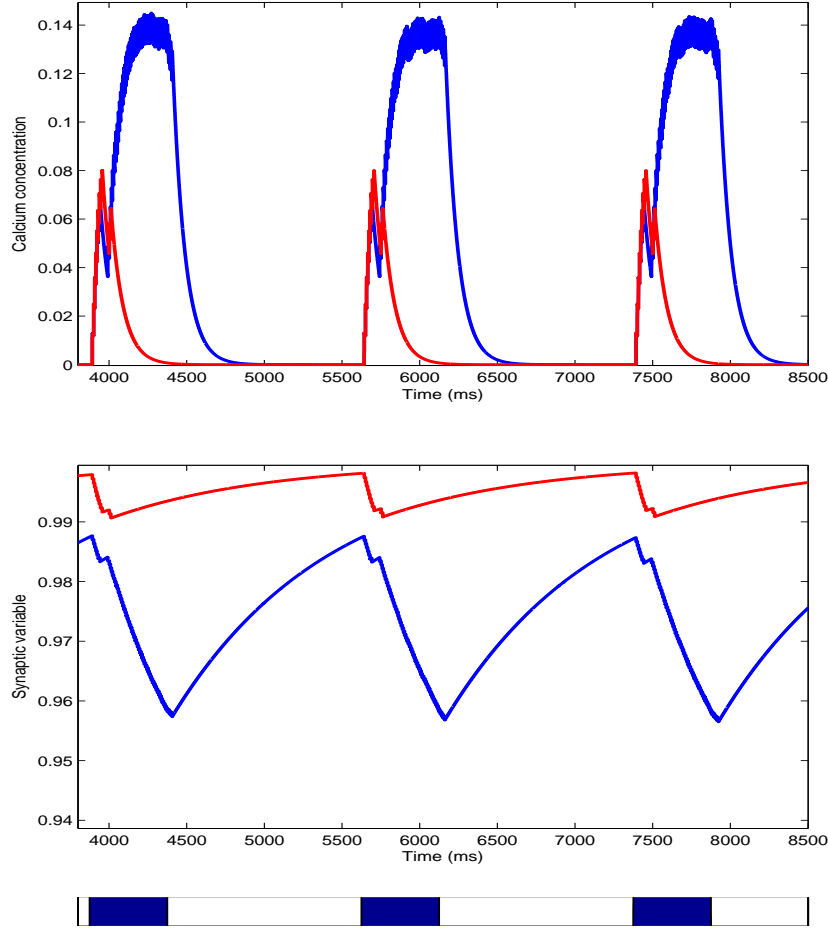


Figure 4.4: Slow variables evolutions for two single neurons during one cycle in the repetition-state. $t_{\text{on}} = 500$, $t_{\text{off}} = 1250$. Blue lines correspond to excitatory neuron 15 from the subpopulation consisting of neurons 1, ..., 30, red lines correspond to excitatory neuron 45 from the subpopulation consisting of neurons 31, ..., 60. (a): calcium evolution, (b) evolution of synaptic variable.

a both-off steady state, a both-on steady state, a one-on steady state and system oscillations. These oscillations correspond with the population analogue of binocular rivalry because activity-levels and calcium-levels fall and drop. Restrictions on the parameters for the stable-states α , β , I_1 and I_2 can be found by looking at the contribution of the heavisides. For example, in order to end up in the all-on state, both activity-levels should converge to 1 and the adaptation-levels to ϕ_a . This happens only if the term $\alpha u_1 g_1 - \beta u_2 g_2 - a_1 + I_1$ is positive, and substituting 1 for the u_i 's and ϕ_a for the a_i 's leads to the restriction $[\alpha - \beta - \phi_a + I_1 > 0, \alpha - \beta - \phi_a + I_2 > 0]$. We find the following restrictions:

$$\text{all-on: } \rightarrow (1, 1, \phi_a, \phi_a) : [\alpha - \beta - \phi_a + I_1 > 0, \alpha - \beta - \phi_a + I_2 > 0] \quad (4.5)$$

$$\text{all-off: } \rightarrow (0, 0, 0, 0) : [I_1 < 0, I_2 < 0] \quad (4.6)$$

$$\text{one-on: } \rightarrow (1, 0, \phi_a, 0) : [\alpha - \beta + I_1 > 0, -\beta + I_2 < 0] \quad (4.7)$$

We included the on-off-cycle by multiplying the input with a block-pulse signal $y(t)$ in the

reduced model (4.1) to obtain a reduced description for the on-off-model:

$$\frac{du_1}{dt} = -u_1 + f(\alpha u_1 - \beta u_2 - a_1 + I_1 \cdot y) \quad (4.8)$$

$$\frac{du_2}{dt} = -u_2 + f(\alpha u_2 - \beta u_1 - a_2 + I_2 \cdot y) \quad (4.9)$$

$$\tau_a \frac{da_1}{dt} = -a_1 + \phi_a f(\alpha u_1 - \beta u_2 - a_1 + I_1 \cdot y) \quad (4.10)$$

$$\tau_a \frac{da_2}{dt} = -a_2 + \phi_a f(\alpha u_2 - \beta u_1 - a_2 + I_2 \cdot y) \quad (4.11)$$

If we define $z(t)$ as a single on-off-cycle in (4.12), $y(t)$ consists of an array of subsequent signals $z(t)$, so $y(t)$ equals 1 during on-durations and 0 during off-durations over the entire sequence of subsequent trials.

$$z(t) = \begin{cases} 1 & \text{if } t < t_{\text{on}}, \\ 0 & \text{if } t > t_{\text{on}}. \end{cases}, t \in [0, t_{\text{on}} + t_{\text{off}}] \quad (4.12)$$

In order to connect (4.8) with the human psychophysics experiments, the network should be able to temporarily operate in the all-off-state during the off-duration, before returning to the oscillatory behavior during on-durations. Since there is no input I_1 or I_2 during the off-durations, restriction (4.8) cannot be met. Including the synaptic population levels and using the full reduced description version changes the restrictions only quantitatively, not qualitatively. In contrast to the Noest model in [24], this reduced description does not allow a successful bifurcation analysis, which could possibly lead to insight in the overall governing dynamics and qualitative changes within the network. Finding a reduced model that produces repetitions and allows bifurcation analysis might provide insight in the parameter-regions that lead to unwanted behavior such as activity-volleys and waves of activity.

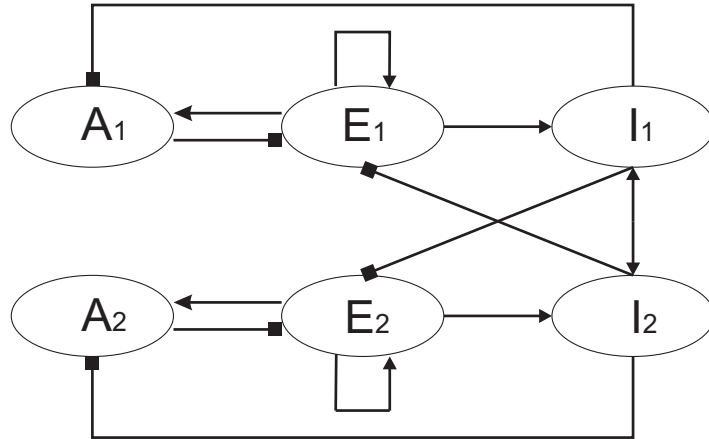


Figure 4.5: Schematic representation implicit-cross-inhibition reduced model. A_i : adaptation units, E_i : excitatory units, I_i : inhibitory units. Arrows indicate excitatory connections and lines with square blocks indicate inhibitory connections.

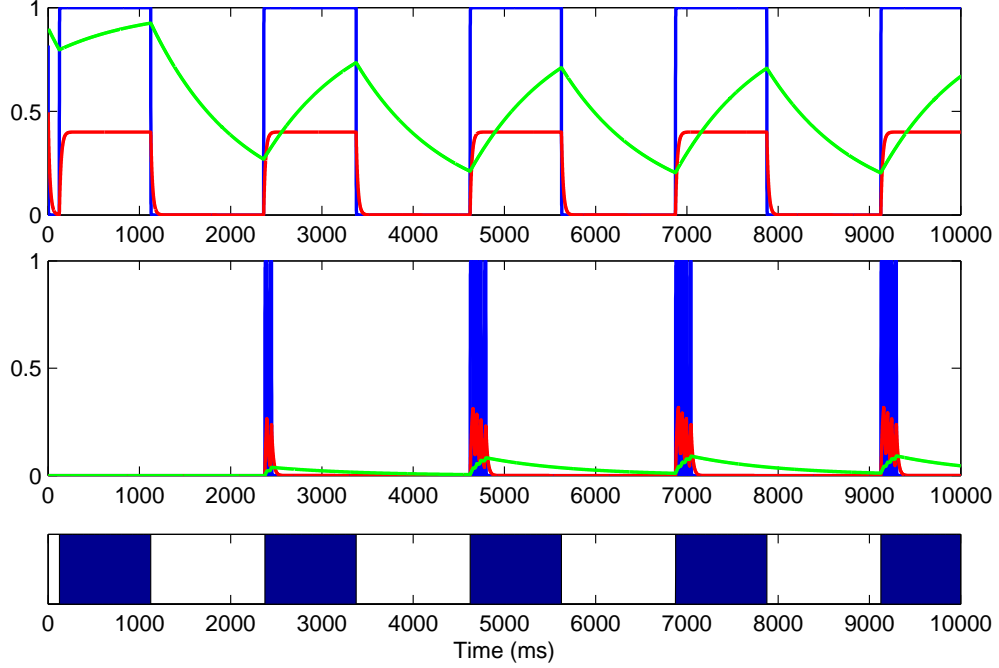


Figure 4.6: Repetitions in the ad hoc reduced model (equations (4.13),... (4.18)) with $\alpha = 0.2$, $\beta = 0.8$, $\gamma = 1$, $\psi = 1$, $t_{\text{on}} = 1000$, $t_{\text{off}} = 1250$, $I = 0.3$, $\tau_a = 20$, $\phi_a = 0.4$, $\tau_i = 1000$, $\phi_i = 1$ and f, g and h heavisides. Activity in population one (on top) shows repeated percepts over the trials, whereas the activity in population two (middle figure) is suppressed. Blue lines correspond to excitatory variables, green lines correspond to inhibitory variables and red line correspond to adaptation variables.

Instead of using self-excitation and direct cross-inhibition, we considered a more elaborate approach in which self-excitation, implicit cross-inhibition and direct excitation occurs with mean-field activity of two populations, where each population consists of an excitatory and inhibitory component. This leads to the following reduced description:

$$\frac{dE_1}{dt} = -E_1 + f(\alpha E_1 - \beta I_2 - A_1 + Iy) \quad (4.13)$$

$$\frac{dE_2}{dt} = -E_2 + f(\alpha E_2 - \beta I_1 - A_2 + Iy) \quad (4.14)$$

$$\tau_a \frac{dA_1}{dt} = -A_1 + \phi_a h(\alpha E_1 - \beta I_2 - A_1 + Iy) \quad (4.15)$$

$$\tau_a \frac{dA_2}{dt} = -A_2 + \phi_a h(\alpha E_2 - \beta I_1 - A_2 + Iy) \quad (4.16)$$

$$\tau_i \frac{dI_1}{dt} = -I_1 + \phi_i g(\gamma E_1 - \psi I_2 + Iy) \quad (4.17)$$

$$\tau_i \frac{dI_2}{dt} = -I_2 + \phi_i g(\gamma E_2 - \psi I_1 + Iy) \quad (4.18)$$

During on-durations one of the populations should dominate the other, leading to $(1, 0, \phi_a, 0, \phi_i, 0)$ or $(0, 1, 0, \phi_a, \phi_i, 0)$. This leads to the following restrictions:

$$\text{dominant percept: } \rightarrow (1, 0, \phi_a, 0, \phi_i, 0) : [\alpha - \phi_a + I > 0, -\beta\phi_i + I < 0, \gamma > 0, -\psi + I < 0] \quad (4.19)$$

n combination with the slower inhibition-evolution, these restrictions provided a starting point for finding alternation patterns within choice-sequences, see figure 4.6. In order to test the data from the neuronal network against our neuronal network, we calculated average firing rates over the subpopulations within the excitatory and inhibitory populations, and compared them with the patterns in the reduced figures. However, without synaptic depression the neuronal network model produces synchronous activity-patterns. This might be due to the fact that the synaptic coupling balance between the excitatory and inhibitory population is very sensitive, so too much excitation probably disturbs the coupling balance and situates the network in the all-on-domain. It should be noted this does not refute a hypothesis that perception of stimulus onset can be induced by calcium-dynamics only, but merely that the current neuronal network configuration does not allow a straightforward way to test this explicitly. In conclusion: although the ad hoc reduced model is able to produce repetitions (with some volley-like synchronous initial behavior, just as we found in the neuronal network activity) with only spike frequency adaptation mediated by calcium-concentrations, it is difficult to see how the reduced model relates to the overall neurobiological mechanisms during stimulus onset.

5 Discussion

In order to develop a neuronal network model for intermittently presented conflicting stimuli, we have used an approach from binocular rivalry studies by Laing and Chow in [18] as our starting point. We first reproduced the model and established the validity by testing it against their main results: the distribution of the dominance duration, the largest Lyapunov exponent and the second Levelt proposition. Since our results provided a satisfactory connection with their results, we extended the basic model by including the on-off-structure. If we assume centralized activity corresponds with the perception of the dominant percept and localized bumps in activity suggest spontaneous switches on a perceptual level, our cortical neuronal network of excitatory and inhibitory neurons with on-off-cycles reproduces human psychophysics results by Klink and Noest. The off-durations crucially determine the networks overall behavior reflected in the choice sequences. Longer off-durations correspond to repetitions whereas shorter off-durations lead to alternations and also more complicated sequences of alternations and repetitions can be generated.

In order to understand the underlying dynamical difference between patterns of alternations, repetition and mixtures, we have tried to analyze a reduced description of the model. The Heaviside-formulation in the reduced description by Laing and Chow does not allow the on-off-model to periodically return to a stable off-state during off-durations, which makes it impossible to directly fine-tune the population model in the biophysical desirable regime. This might be explained by Noest in [24], since this reduced model uses the neural outputs as the primary dynamical variables. Given the thresholded sigmoidal shape of neural firing-rate functions, this makes this approach blind to a subthreshold side effect of unequal adaptation that Noest identifies as sufficient for producing the percept-choice phenomena. Using the mean-field approach employed by Wang and Wong might lead to a reduced model with the necessary bias-mechanism to allow repetitions and allow bifurcation analysis. It is an interesting question on its own to see how the models by Wang and Wong relate to our neuronal network model (or the model by Laing and Chow in general) since they differ significantly in population-size and biological properties.

We formulated an ad hoc reduced description with self-excitation, implicit cross-inhibition and direct excitation. Although the ad hoc reduced model is able to produce repetitions (with some volley-like synchronous initial behavior, which was exactly what we found in the neuronal network activity) with only spike frequency adaptation mediated by calcium-concentrations, it is difficult to see how the reduced model relates to the overall neurobiological mechanisms during stimulus onset. Hence it is difficult to refute any hypothesis concerning the necessity of spike frequency adaptation or the redundancy of synaptic depression to describe the dynamics during stimulus onset of sequences of conflicting stimuli within our current neuronal network formulation, since we cannot disconnect the two slow processes and it is unclear how Laing and Chow have chosen their coupling-strengths.

Before different reduced approaches should be taken into account, we expect a comparison with the neuronal network data and the statistical analysis by Klink on his neurophysiological data-set might provide insight in the validity of the connection between the micro-level of our network model and the macro-level of percept sequences. By analyzing the neuronal data with the same tools as Klink used in his neurophysiological approach, the model can be tested against his neuronal stabilization hypothesis. A first exploration of the fano factor did not reveal direct similarities, but an in-depth analysis of the spike-data will lead to insight in the overall relation between the macro-level of perceptions and the micro-level of neuronal

responses. We expect the patterns found in our neuronal network model are more explicit than the effects found by Klink, since our model does not include pre-stage adaption or noise.

After this comparison on the neuronal level, we can focus on formulating a more structural reduced approach that allows bifurcation analysis, such as the approaches by Wang and Wong, Noest and Laing et al. in [28, 24, 19]. Furthermore, neurobiological experiments involving techniques such as calcium-imaging can provide alternative evidence for the biophysical mechanisms underlying percept sequences during experiments with an on-off-structure. The neuronal network model can be improved by taking these results into account, leading to a more biophysical model and elimination of unwanted patterns such as volleys or waves of activity. We believe such an interdisciplinary approach, combining results neurobiological experiments with mathematical analysis on both scales, might be the key to successfully understand and describe perceptual decision making.

References

- [1] Abbott, L.F., Varela, J.A., Kamal Sen, Nelson, S.B., *Synaptic Depression and Cortical Gain Control*, Science 275: 220-224, 1997
- [2] Alais, D., Blake, R. , *Binocular rivalry.*, Cambridge, USA: MIT Press., 2004
- [3] Brascamp, J.W., Pearson, J., Blake, R., van den Berg, A.V., *Intermittent ambiguous stimuli: Implicit memory causes periodic perceptual alternations*, Journal of Vision 9(3):3, 1-23, 2009
- [4] Brunel, N., Wang, X.J., *Effects of neuromodulation in a cortical network model of object working memory dominated by recurrent inhibition*, Journal of Computational Neuroscience 11: 63-85, 2001
- [5] Cho, R., Nystrom, L., Brown, E., Jones, A., Braver, T., Holmes, P., et al., *Mechanisms underlying dependencies of performance on stimulus history in a two-alternative forced-choice task*, Cognitive, Affective and Behavioral Neuroscience, 2, 283-299, 2002
- [6] Churchland, M.M. et al, *Stimulus onset quenches neural variability: a widespread cortical phenomenon*, Nature Neuroscience 13: 369-378, 2010
- [7] Dayan, P., Abbott, L.F., *Theoretical Neuroscience: Computational and Mathematical Modeling of Neural Systems*, The MIT Press, 2001
- [8] Ermentrout, G.B., *Neural networks as spatio-temporal pattern forming systems*, Rep. Prog. Phys. 61: 353-430., 1998
- [9] Furstenaus, N., *Computational Nonlinear Dynamics Model of Percept Switching with Ambiguous Stimuli*. Lecture Notes in Computer Science, Volume 5620/2009, 227-236, 2009
- [10] Gao, J., Wong-Lin, K.F., Holmes, P., Simen, P., Cohen, J.D., *Sequential Effects in Two-Choice Reaction Time Tasks: Decomposition and Synthesis of Mechanisms*, Neural Computation 21: 2407-2436, 2009
- [11] Huk, A.C., Shadlen, M.N., *A neural integrator underlying perceptual decision-making in macaque parietal cortex*, Journal of Neuroscience 25: 10420-10436, 2005
- [12] Izhikevich, E.M., *Dynamical systems in a neuroscience: the geometry of excitability and bursting*, MIT Press, 2005
- [13] Kantz, H., *A robust method to estimate the maximal Lyapunov exponent of a time series*, Phys. Lett. A 185, 77, 1994
- [14] Kavanau, J.L., *Memory, sleep, and dynamic stabilization of neural circuitry: evolutionary perspectives*, Neuroscience and Biobehavioral Reviews 20(2): 289-311, 1996
- [15] Kirby, N., *Sequential effects in two-choice reaction time: Automatic facilitation or subjective expectancy?*, Journal of Experimental Psychology: Human Perception and Performance, 2, 567-577, 1976

-
- [16] Klink, P.C., van Ee, R., Nijs, M.M., Brouwer, G.J., Noest, A.J., van Wezel, R.J.A., *Early interactions between neuronal adaptation and voluntary control determine perceptual choices in bistable vision*, Journal of Vision 8(5):16, 1-18 2008
- [17] Klink, P.C., Oleksiak, A., Lankheet, M.J.M., van Wezel, R.J.A., *Upcoming: Intermittent stimulus presentation stabilizes neuronal responses in macaque area MT*, 2011
- [18] Laing C.R., Chow C.C., *A Spiking Neuron Model for Binocular Rivalry*, Journal of Computational Neuroscience 12: 39-53, 2002
- [19] Laing C.R., Frewen T., Kevrekidis I.G., *Reduced Models for Binocular Rivalry*, Journal of Computational Neuroscience 28: 459-476, 2010
- [20] Leopold D.A., Wilke M., Maier A., Logothetis N.K., *Stable perception of visually ambiguous patterns.*, Nature Neuroscience 5:605-609, 2002
- [21] Logothetis, N.K., Leopold, D.A., Sheinberg, D.L. , *What is rivalling during binocular rivalry?*, Nature 380: 621-624, 1996
- [22] Maimon, G., Assad, J.A., *Beyond Poisson: increased spike-time regularity accross primate parietal cortex*, Neuron 62: 426-440, 2009
- [23] McCormick, D.A., Huguenard J.R., *A Model of the Electrophysiological Properties of Thalamocortical Relay Neurons*, Journal of Neurophysiology 68(4): 1384-1400, 1992
- [24] Noest, A.J., van Ee, R., Nijs, M.M., van Wezel, R.J.A., *Response of neurons in the lateral intraparietal area during a combined visual discrimination reaction time task*, Journal of Vision 7(8):10, 1-14, 2007
- [25] Roitman, J.D., Shadlen, M.N., *Percept-choice sequences driven by interrupted ambiguous stimuli: A low-level neural model*, Journal of Neuroscience 22: 9475-9489, 2002
- [26] Soetens, E., Boer, L., Hueting, J., *Expectancy or automatic facilitation? Separating sequential effects in two-choice reaction time*, Journal of Experimental Psychology: Human Perception and Performance, 11, 598-616, 1985
- [27] Wang, X.J., *Probabilistic Decision Making by Slow Reverberation in Cortical Circuits* Neuron 36: 955-968, 2002
- [28] Wong, K., Wang, X.J., *A Recurrent Network Mechanism of Time Integration in Perceptual Decisions* The Journal of Neuroscience 26(4):1314-1328, 2006

6 Appendix

Functions in Laing and Chow:

$m_{\text{inf}}(V)$	$= \frac{\alpha_m(V)}{\alpha_m(V) + \beta_m(V)}$
$\alpha_m(V)$	$= \frac{0.1(V+30)}{1 - e^{-0.1(V+30)}}$
$\beta_m(V)$	$= 4e^{-\frac{(V+55)}{18}}$
$\alpha_n(V)$	$= \frac{0.01(V+34)}{1 - e^{-0.1(V+34)}}$
$\beta_n(V)$	$= 0.125e^{-\frac{-(V+44)}{20}}$
$\alpha_h(V)$	$= 0.07e^{-\frac{-(V+44)}{20}}$
$\beta_h(V)$	$= \frac{1}{1 + e^{-0.1(V+14)}}$
σV	$= \frac{1}{1 + e^{-\frac{-(V+20)}{4}}}$
g_{ee}^{jk}	$= \alpha_{ee} \sqrt{\frac{50}{\pi}} e^{-50 \left[\frac{j-k}{N} \right]^2}$
g_{ie}^{jk}	$= \alpha_{ie} \sqrt{\frac{20}{\pi}} e^{-20 \left[\frac{j-k}{N} \right]^2}$
g_{ei}^{jk}	$= \alpha_{ei} \sqrt{\frac{20}{\pi}} e^{-20 \left[\frac{j-k}{N} \right]^2}$
g_{ii}^{jk}	$= \alpha_{ii} \sqrt{\frac{30}{\pi}} e^{-30 \left[\frac{j-k}{N} \right]^2}$

Constants in Laing and Chow:

g_L	$= 0.05$
V_L	$= -65$
g_K	$= 40$
V_K	$= -80$
g_{Na}	$= 100$
V_{Na}	$= 55$
V_{Ca}	$= 120$
g_{AHP}	$= 0.05$
ψ	$= 3$
τ_e	$= 8$
τ_g	$= 1000$
f	$= 1.1$
τ_i	$= 10$
V_{ee}	$= 0$
V_{ie}	$= -80$
V_{ei}	$= 0$
V_{ii}	$= -80$
α_{ee}	$= 0.285$
α_{ie}	$= 0.36$
α_{ei}	$= 0.2$
α_{ii}	$= 0.07$